Ore Geology Reviews 85 (2017) 107–130

Contents lists available at ScienceDirect

Ore Geology Reviews

journal homepage: www.elsevier.com/locate/oregeorev

Tube fossils from gossanites of the Urals VHMS deposits, Russia: Authigenic mineral assemblages and trace element distributions

N.R. Ayupova [a,b,*], V.V. Maslennikov [a,b], S.G. Tessalina [c], O.P. Shilovsky [d], S.A. Sadykov [a], S.P. Hollis [e], L.V. Danyushevsky [f], N.P. Safina [a], E.O. Statsenko [d]

[a] Institute of Mineralogy, Uralian Branch of RAS, Miass 456000, Russia
[b] South Urals State University, Department of Geology, October Ave. 16,Miass 456318, Russia
[c] John de Laeter Centre for Isotope Research, Curtin University, Kent St., Bentley 6102, WA, Australia
[d] Kazan Federal University, 18 Kremlyovskaya St., Kazan, 420008, Russia
[e] Irish Centre for Research in Applied Geosciences (iCRAG), University College Dublin, Belfield, Dublin 4, Ireland
[f] University of Tasmania, CODES, Hobart 7000, Tasmania, Australia

ARTICLE INFO

Article history:
Received 16 December 2015
Received in revised form 29 July 2016
Accepted 3 August 2016
Available online 6 August 2016

Keywords:
Tube microfossils
Bacterial and fungi forms
Gossanites
VHMS deposits
Urals

ABSTRACT

The occurrence, types, morphology, and mineralogical characteristics of tube microfossils were studied in gossanites from twelve VHMS deposits of the Urals. Several types of tube microfossils were recognized, including siboglinids, polychaetes and calcerous serpulids, replaced by a variety of minerals (e.g. hematite–quartz, hematite–chlorite, carbonate–hematite) depending on the nature of the substrate prior to the formation of the gossanites. Colonial hematite tube microfossils (~150 μm across,1–2 mm long) are composed of hematitic outer and inner walls, and may exhibit a cellular structure within their cavities. Spherical forms are saturated with Fe-oxidizing bacteria inside the tubes – probably analogues of trophosomes. Colloform stromatolitic outer wall surfaces are characterized by the presence of numerous interlaced filaments of hematite (2–3 μm diameter, up to 1–2 mm long). Between tube microfossils, the hematitized cement contains bundles of hematitized filaments with structures similar to the hyphae of fungi. Hematite–chlorite tube microfossils are scattered in gossanites, mostly as biological debris. They are typically 30 to 300 μm in diameter and 1 to 5 mm long. The layered structure of their tube walls is characterized by hematite–quartz and chlorite layers. Abundant filamentous bacteria coated by glycocalix and chlorite stromatolite are associated with hematite–chlorite tubes. The carbonate–hematite tube microfossils (up to 300 μm across, 2–3 mm long) occur in carbonate-rich gossanites. The tubes are characterized by fine (~10 μm thick) walls of hematite and cavities dominated by relatively dark carbonate or hematite. Carbonates may be present both in walls and cavities. Stromatolite-like leucoxene or hematite–carbonate aggregates were also found in association with tubes. Randomly oriented filaments are composed of ankerite. Single filaments are composed of individual cells, typically smaller than 100 nm across, similar to that of magnetotactic bacteria.

Three dimensional tomographic images of all types of tube microfossils demonstrate a clear wavy microlayering from outer and inner walls, which may reflect segmentation of the tube worms. The traces of burrowing or fragments of glycocalix with relict spheres are typical of tube microfossils from gossanites.

The carbon isotopic composition of carbonates associated with tube microfossils from hematite–quartz, hematite–carbonate, and hematite–chlorite gossanites average − 7.2, − 6.8, −22.8‰, PDB, respectively. These values are indicative of a biogenic origin for the carbonates. The oxygen isotopic composition of these carbonates is similar in all three gossanite types averaging + 13.5, + 14.2, + 13.0‰ (relative to SMOW), and indicative of active sulfate reduction during the diagenetic (and anadiagenetic) stages of the sediments evolution. The trace element characteristics of hematite from tube microfossils are characterized by high contents of following trace elements (average, ppm): Mn (1529), As (714), V (540), W (537), Mo (35), and U (5). Such high contents are most likely the result of metal and metalloid sorption by fine particles of precursor iron hydroxides during the oxidation of sulfides and decomposition of hyaloclasts via microbially-mediated reactions.

* Corresponding author at: Institute of Mineralogy, Uralian Branch of RAS, Miass 456000, Russia.
E-mail address: aupova@mineralogy.ru (N.R. Ayupova).

http://dx.doi.org/10.1016/j.oregeorev.2016.08.003
0169-1368/

1. Introduction

Numerous volcanic-hosted massive sulfide (VHMS) deposits worldwide are spatially associated with silica–iron-rich (silica–hematite) rocks (e.g., Constantinou and Govett, 1973; Kalogeropoulos and Scott, 1983; Herzig et al., 1991; Duhing et al., 1992; Peter and Goodfellow, 1996; Grenne and Slack, 2003; Maslennikov et al., 2012; Tornos et al., 2015). These rocks are described under a variety of names in VHMS literature, such as: Algoma-type iron formations, silica–iron exhalites, jaspers, tuffites, tetsusekiei, ochres, jasperites, gossanites, umbers, vasskis (e.g., Hollis et al., 2015), and are comparable with deep-sea hydrothermal iron–oxide deposits from the modern ocean (e.g., Adachi et al., 1986; Alt, 1988; Herzig et al., 1991; Hekinian et al., 1993; Halbach et al., 2002). Although a variety of models for the formation of these rocks have been proposed, recent studies have highlighted that the metabolic activity of bacteria and fungi play an important role in their genesis (Juniper and Fouquet, 1988; Hannington and Jonasson, 1992; Duhing et al., 1992; Emerson and Moyer, 2002; Grenne and Slack, 2003; Little et al., 2004).

Fe-oxide bacteriogenic textures with a wide variety of morphologies have been found in Devonian silica–iron-rich rocks from VHMS deposits of the Urals (Ayupova and Maslennikov, 2012, 2013). The formation of these rocks has been attributed to halmyrolysis (i.e., seafloor weathering) of clastic sulfide sediments or plume settled sulfide particles, which were mixed with background sediments (i.e., hyaloclastites and/or their calcareous varieties) (Maslennikov et al., 2012). Such rocks are termed “gossanites” (Maslennikov et al., 2012) due to their similarities with submarine gossans (Hannington et al., 1988; Herzig et al., 1991). Locally, gossanites form dispersion halos around eroded sulfide mounds, covering an area twice to several times that of the orebodies themselves, and may be used as a proxy to mineralization (Ayupova et al., 2011; Maslennikov et al., 2012; Ayupova et al., 2015). Diverse species of bacteriogenic filaments suggest that microbial activity played an important role in sulfide oxidation and the destruction of volcanic glass.

The discovery of hematitized tube microfossils in gossanites from the Urals is of special interest, as they indicate effective biological mechanisms for the precipitation of authigenic minerals and the accumulation of some trace elements (e.g., Ayupova et al., 2016). Due to only low grades of metamorphism, their preservation style is similar to that of polychaete vent fossils in massive sulfide ores containing black smoker chimney fragments (e.g., Little et al., 1999).

In this paper, we review the occurrence of tube fossils, their types, morphology, mineralogy and geochemistry, as well as the bacteria or fungi associated with these fossil assemblages. We also discuss the contribution of biogenic and abiogenic components to the accumulation of metals and metalloids in gossanites from VHMS deposits.

2. Geological outline

2.1. Geological background

The Urals fold belt is subdivided into several structural zones (Fig. 1), which represent different tectonic settings, including fragments of island arcs (Tagyl in the north and West, and East Magnitogorsk in the south), inter-arc (Sibai) and back-arc (Dombarovka, West Mugodzhary, Rezh) basins, as well as a possible marginal sea (Sakmara) (e.g., Prokin and Buslaev, 1999; Zaykov et al., 2002; Herrington et al., 2005). VHMS deposits formed in all these tectonic environments from the Late Silurian to Middle Devonian (Prokin and Buslaev, 1999).

Samples for our study were collected from the Novo-Shemur, Uchaly, Talgan, Molodezhnoye, XIX Parts'ezd, Uzelga, Alexandrinskoye, Babaryk, Sibai, Yaman-Kasy, Blyava, and Priorskoye VHMS deposits (Fig. 1). The Novo-Shemur deposit is located in the northern part of the Tagyl arc and hosted by a Silurian andesite–dacite complex (Prokin and Buslaev, 1999). VHMS deposits of the East Magnitogorsk arc (Uchaly, Talgan, Molodezhnoye, XIX Parts'ezd, Uzelga, Alexandrinskoye, Babaryk) and Sibai inter-arc basin (Sibai) occur within rhyolite–basaltic complexes of the Middle Devonian Karamalytash Formation (Zaykov et al., 2002; Herrington et al., 2005). The Yaman-Kasy and Blyava deposits are located within the Sakmara marginal sea and hosted by a Silurian basalt–rhyolite sequence (Zaykov, 2006). The Priorskoye VHMS deposit is localized in the Dombarovka–Mugodzhary back-arc basin, with mineralization occurring in differentiated volcanic rocks of the Karamalytash Formation at the contact of basalts with rhyodacites (Prokin and Buslaev, 1999).

The most comprehensively studied VHMS deposits of the Urals have been interpreted as variously eroded sulfide mounds (Maslennikov, 2006) (Fig. 2). Destruction of smoker chimneys was followed by submarine weathering and slumping of fragmental ore material onto the paleoseafloor. Coarse clastic sulfide breccias are abundant on the slopes of the orebodies, whereas sulfide turbidites occur on the flanks of the deposits (Fig. 2). The clastic sulfide ores of the Yaman-Kasy, Talgan, Molodezhnoye, Uzelga, Alexandrinskoye, and Sibai deposits contain fragments of black smoker chimneys and diffusers (Maslennikov, 2006; Maslennikova and Maslennikov, 2007; Maslennikov et al., 2013; Maslennikov et al., 2017–in this issue). Hydrothermal vent fossils, which include small to giant vestimentiferans and numerous polychaete tube fossils, were found in the life position or as redeposited fragments in association with black smoker chimneys (Maslennikov, 1999; Little et al., 1999; Zaykov, 2006). Fragments of small pyritized tube fossils are present inside the ore clasts or as individual clasts in sulfide turbidites at the flanks of the ore bodies. Single hematitized tube microfossils occur in gossanite layers, which typically crown the massive sulfide orebodies and may be intercalated with sulfide turbidite sand hyaloclastites on the flanks of some deposits (Zaykov, 2006; Ayupova et al., 2016).

2.2. Characteristics of gossanites

The main lithological and mineralogical characteristics of gossanites from the studied VHMS deposits are described in Maslennikov et al. (2012), and briefly summarized here. Gossanites contain a wide variety of textures and mineral assemblages owing to the different proportion of primary sulfide, hyaloclastite, and carbonate components. Using their dominant mineralogy, the samples were divided into three groups: hematite–quartz, hematite–chlorite, and hematite–carbonate.

The replacement of sulfides and hyaloclasts by hematite–quartz aggregates are recognized in hand specimens of the Fe-rich (Fe_2O_3 up to 30 wt.%) hematite–quartz (or hematite) gossanites. The content of Al_2O_3 is very low (up to 5 wt.%) as a result of complete hematitization of hyaloclasts. These rocks are often enriched in TiO_2 (up to 0.48 wt.%). Alteration of hyaloclasts led to the formation of Ti-rich areas due to the precipitation of anatase after the complete hematitization of hyaloclasts. Chalcopyrite, galena and barite, and rare native gold and coloradoite, represent more stable authigenic mineral assemblages and occur in hematite–quartz pseudomorphs after sulfide clasts, and as rare individual grains in the hematite–quartz cement.

The hematite–chlorite gossanites contain relict sulfides, with very high Fe_2O_3 (up to 48 wt.%) and Al_2O_3 (up to 18 wt.%) contents due to the formation of pure hematite pseudomorphs after sulfides and preservation of hyaloclasts. These gossanites are composed predominantly of chlorite, quartz, and hematite, with accessory rutile, barite, apatite, chalcopyrite and sphalerite. The replacement of albite by chlorite, and destruction of Ti-magnetite concomitant with the appearance of rutile, are the most obvious effects of alteration on the mixed sulfide–hyaloclastic sediments. Rare native gold, Hg-, Au-, Ag-tellurides, selenides, and cassiterite are associated with authigenic chalcopyrite, bornite, tennantite, digenite and sphalerite (Ayupova et al., 2015).

The hematite–carbonate gossanites (Fe_2O_3 up to30 wt.%) are red–brown ferruginous rocks with high amount of carbonates (Mn-calcite,

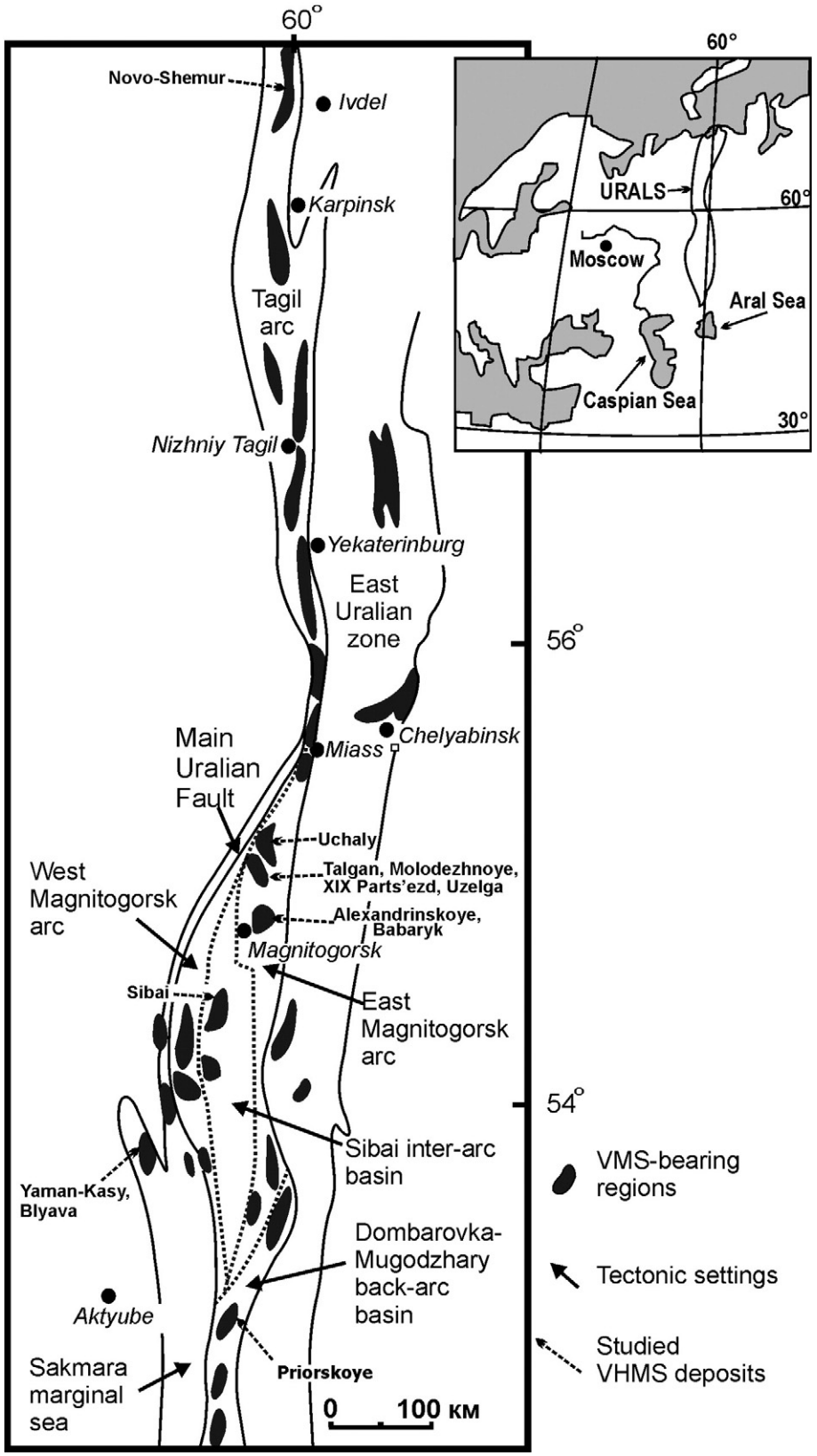

Fig. 1. VHMS-bearing regions of the Urals and position of the studied deposits (based on Prokin and Buslaev, 1999; Zaykov et al., 2002; Herrington et al., 2005).

ankerite, siderite, dolomite), variable amount of hematite, silica, chlorite, and carbonates, rare hematite–quartz pseudomorphs after sulfides, and authigenic chalcopyrite, galena, crystalline pyrite and pyrite nodules. The CaO content in these rocks reaches 24 wt.%. Carbonate and iron–oxide mineralization is typically accompanied by authigenic pseudomorphic apatite after carbonates and volcanic glass. Titaniferous magnetite or leucoxene also occurs in the fine-clastic hematitized matrix.

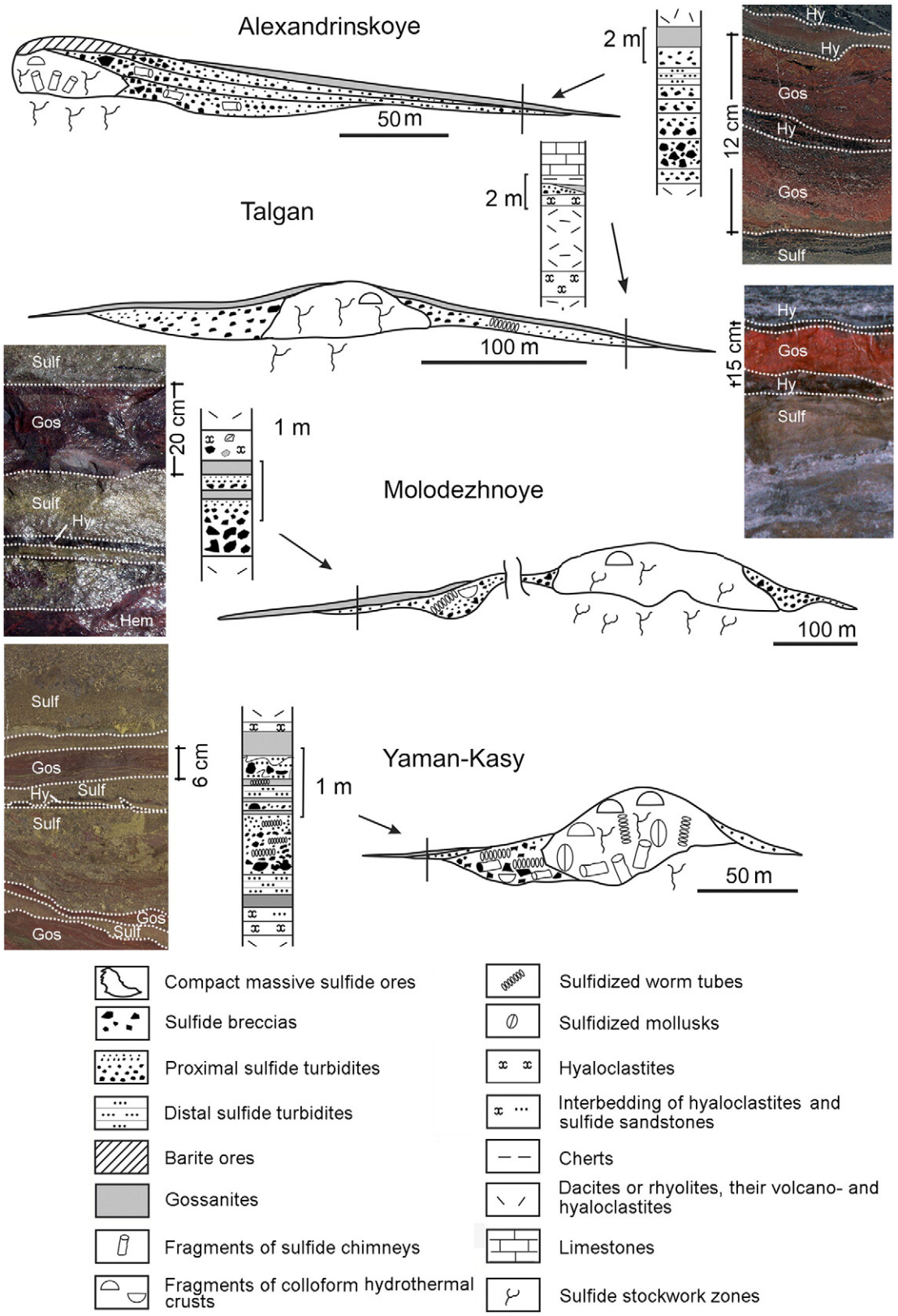

Fig. 2. Position of gossanites (Gos) intercalated with sulfide turbidites (Sul) and hyaloclastites (Hy) at the flanks of massive sulfide orebodies of some VHMS deposits (modified after Maslennikov et al., 2012).

2.3. Sampling

Samples of gossanites with tube microfossils were collected from open pits and underground mines of the Priorskoye, Yaman-Kasy, Blyava, Sibai, Alexandrinskoye, Babaryk, Molodezhnoye, Talgan, Uzelga, XIX Parts'ezd, Uchaly and Novo–Shemur VHMS deposits. Sixty polished slabs varying in size from 5 × 5 up to 30 × 40 cm were studied macroscopically.

3. Analytical methods

3.1. Microscopy studies

About 100 polished sections were made from different serial sections (transverse, longitudinal, and oblique) of the polished slabs to study the internal structure and mineralogy of the tube fossils. The polished sections were studied by transmitted, reflected light, and dark-field microscopy on an Olympus BX51 microscope at the Institute of Mineralogy, Urals Branch, Russian Academy of Sciences (IMin UB RAS, Miass). The high-resolution textural, morphometric, and elemental (wt.%) analyses of the tube fossils were carried out using an AURIGA CrossBeam SEM equipped with an INCA X-MAXEDS at the Institute of Geology and Petroleum Technologies in the Kazan Federal University (IGPT KFU, Kazan). EDS analyses were carried out using a 1 μm electron beam, 15 nA beam current, 20 kV accelerating voltage, and a counting time of 120 s for each peak.

3.2. X-ray computer tomography

X-ray computer tomography (CT) is well-known non-destructive technique to visualize and quantify the structure of paleontological objects in three dimensions (3D) (Kenter, 1989). The X-ray computer tomography of gossanite samples (27 × 26 × 6 mm in size) from the Talgan, Molodezhnoye and Alexandrinskoye deposits was performed on a PhoenixV|tome|XS 240 industrial X-ray tomograph equipped by a 180 kV/15 W high-power nanofocus X-ray tube and a 240 kV/320 W microfocus tube at the IGPT KFU. Our samples were studied with a microfocus tube at an accelerating voltage of 120 kV, a beam current of 150 mA, and a resolution of 33.4 μm (the volume of 1 voxel) using a Cu filter 0.5 mm thick. Photo- and video-images were taken in the VG Studio MAX 2.1 and Avizo Fire 7.1 program software (Appendix A).

3.3. Stable isotopes (C–O) analysis

Samples of carbonates associated with tube microfossils in gossanite layers, carbonate clasts and hanging-wall limestones were drilled with a diamond microdrill. The carbon and oxygen isotopic composition of carbonates from studied deposits (reported as $\delta^{13}C‰$ relative to PDB and $\delta^{18}O‰$ relative to V-SMOW) were analyzed with a Delta + Advantage, Thermo-Finningan mass-spectrometer using NBS-18, NBS-19, and IAEA-C-3 standards at the IMin UB RAS. The analytical error is ±0.1‰. Results were processed using the ISODAT-2.0 program.

3.4. Trace elements analysis

Quantitative LA–ICP–MS analysis of hematite from gossanites was carried out for trace element characterization (Ti, V, Mn, Cu, Zn, As, Se, Mo, Sb, Te, W, Pb, U, and Tl) on a New Wave 213-nm solid-state laser microprobe coupled to an Agilent 4500 quadrupole ICP-MS housed at the CODES LA–ICP–MS analytical facility, University of Tasmania (Hobart). The analyses were performed by ablating spots ranging in size from 40 to 60 μm. The analysis time for each spot was 100 s, comprising a 30-s measurement of background (laser off) and a 70-s measurement with laser on. Iron was used as the internal standard for quantification of pyrite. An in-house Li-borate fused glass of pyrite was used as the primary calibration standard. The standard was analyzed with a 100-μm beam at 10 Hz. Additional details of the analyses can be found in Danyushevsky et al. (2011).

4. Results

4.1. Tube microfossils: morphological, textural, and geochemical features

All tube microfossils observed are very small and extremely difficult to recognize in either outcrop or core samples with the naked eye. In polished sections, tube microfossils are readily identified in the hematite–quartz matrix by their clear contours. As discussed previously, according to gossanite-type three mineralogical groups may be distinguished: (i) hematite (or fine hematite–quartz intergrowths), (ii) hematite–chlorite, and (iii) carbonate–hematite. They are characterized by specific morphological and textural–structural peculiarities together with different bacteria and fungi assemblages.

4.1.1. Hematite tube microfossils

Hematite microfossils are straight parallel thin tubes approximately 150 μm across and 1 to 2 mm long. They are observed at some distance from each other (intransverse section), in clusters, which represent a colony (Fig. 3a). Locally, one can observe symmetrical round forms at the tube ends, which could represent the mineralized soft tissue of the tube worms (Fig. 3b-c). Tubes are composed of well-distinguishable outer and inner walls, and a cavity (Fig. 3b-e). The outer walls are typically < 10 μm thick, and thinner than the inner walls (~15–20 μm thick). Some tubes have outer walls composed of hematite and inner walls composed of fine intergrowths of hematite and quartz (Fig. 3c), whereas other tube fossils consist entirely of hematite (Fig. 3d, e). Tubes are also characterized by segmentation (Fig. 3e). In the case of complete hematitization, the outer and inner walls have merged with the cavity (Fig. 3f). Hematite from the outer wall is extremely fine, scaly, and curved (Fig. 3g, h). The cavity of the tubes is filled with colloform, gel-like, acicular, and granular hematite and/or quartz (Fig. 3). Rarely, cavities host aggregates of flaky bluish white leucoxene in a quartz cement or chalcopyrite. The composition of hematite is shown in Table 1. It contains Al_2O_3 (0.37–1.51 wt.%), SiO_2 (0.60–2.78 wt.%), and CaO (0.26–1.52 wt.%) and, locally, MnO (0.31–0.55 wt.%), MgO (0.11–0.88 wt.%) and P_2O_5 (0.39–0.56 wt.%).

The tubes in some gossanite layers are very well-preserved and exhibit a cellular structure in the cavity (transverse section; Fig. 4a, b). The cells have spherical forms with a standard diameter of ~9 μm (Fig. 4c), and consist of numerous nanocrystals of hematite with similar orientation (Fig. 4d). The outer surface of the tubes has a patchy, discontinuous veneer of colloform, laminated hematite or finely dispersed hematite–quartz aggregates, which resemble colloform stromatolitic structures (Fig. 4e). The areas with stromatolitic structures are characterized by the presence of numerous interlaced filaments of hematite with diameter of 2–3 μm and length up to 100 μm (Fig. 4f). In such areas, the contours of the tube microfossils are poorly preserved. Between the tubes, the hematitized cement of gossanites contains bundles of hematitized filaments characterized by nuclear structure similar to hyphae of fungi (Fig. 4g). The traces of burrowing or fragments of glycocalix with relict spheres are easily identified in hematitized hyaloclasts (Fig. 4h).

These tubes are typical of the hematite–quartz gossanites with pseudomorphic hematite–quartz aggregates after sulfide clasts and hyaloclasts, which are abundant in the Talgan, Priorskoye, Novo–Shemur, Uchaly, Blyava and Yaman-Kasy VHMS deposits. In these gossanites, the sulfide clasts are fully oxidized and the hyaloclasts are hematitized and surrounded by filaments.

4.1.2. Hematite–chlorite tube microfossils

The hematite–chlorite tube microfossils display round transverse and tubular longitudinal sections, and are typically found scattered in gossanites mostly as biological debris. Locally, some may be preferentially oriented in particular gossanite layers. The tube microfossils are typically 30 to 300 μm in diameter and 1 to 5 mm long. One tube end is always closed, and thicker than the other. The outer and inner surfaces of the tubes are also slightly wavy (Fig. 5a).

The very fine walls of the tube fossils often display a layered structure represented by an intercalation of fine hematite–quartz and chlorite layers (Fig. 5b). Locally, the mineralized soft tissue can be interpreted as a secondary cavity of the body (coelom) similarly to Annelida (Rieger and Purschke, 2005). This feature is visible in the

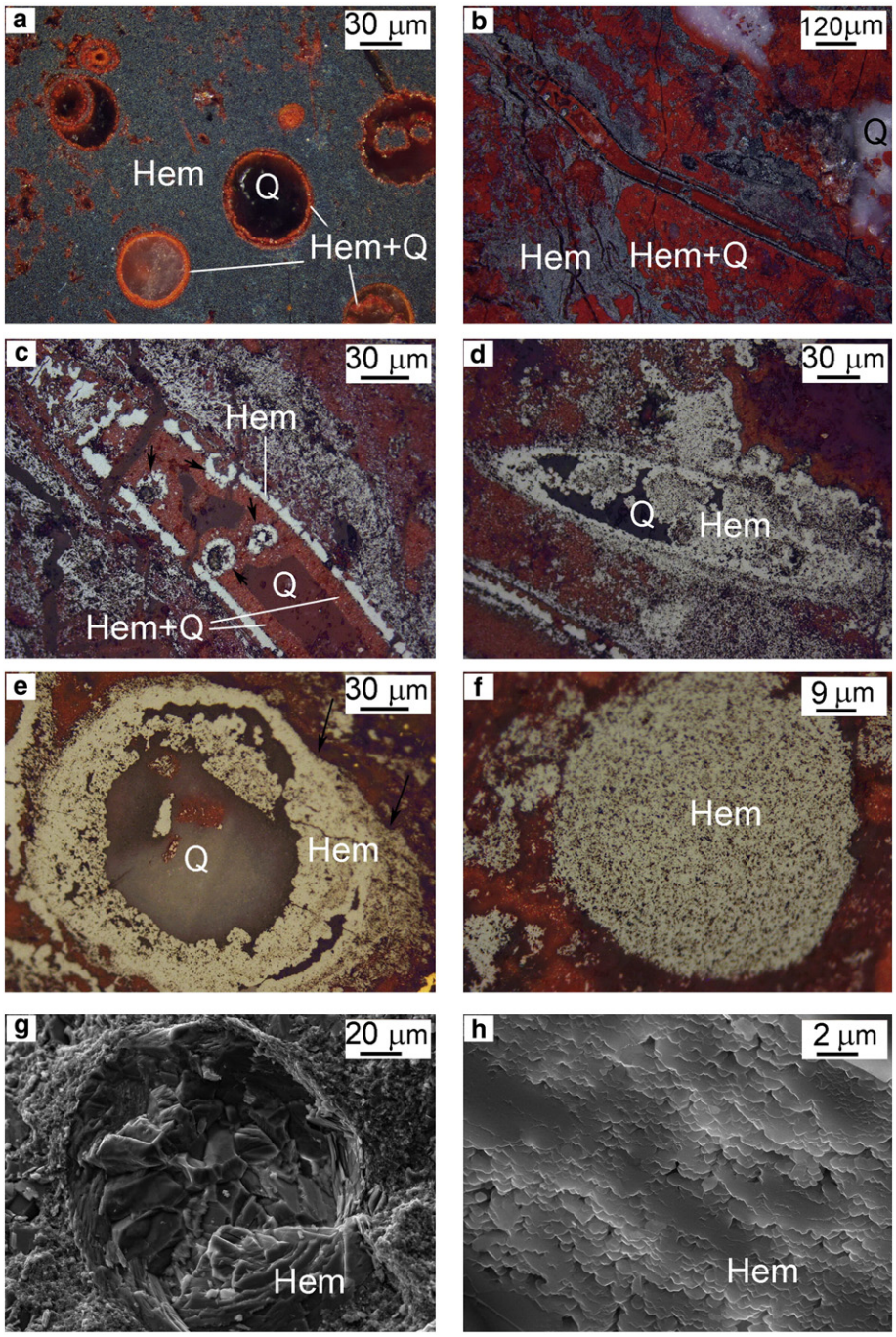

Fig. 3. Hematite tube microfossils: a – colony of the tubes; b – longitudinal section of the tube; c – outer wall composed of hematite, inner wall made up of finely dispersed hematite–quartz aggregates, and symmetrical zonal round forms in the end of the tube, most likely, represented the soft tissue of the tube worms (detail of Fig. 3b); d – oblique cross-section of the tube: the wall is composed of fine-crystalline hematite and the cavity is filled with colloform–nodular hematite; e – the wall incrusted by crystalline hematite and the cavity filled with quartz; arrows indicate segmentation of the tube; f – completely hematitized tube; g – fine-scaly hematite wall of the tube and more compact hematite–quartz material in the cavity overgrown by bacteria; h – fine-scaly hematite of the tube wall (detail of Fig. 3g). Here and Fig. 4: Hem – hematite, Q – quartz, Hem + Q – hematite–quartz aggregates. Dark-field images (a–d), reflected light (e, f) and SEM-photo (g, h). Talgan (a, b, c, e, g, h) and Priorskoye (d, f) deposits.

transverse sections of the tubes (Fig. 5c). Round or oval forms inside the coelom may be interpreted as a digestive tract and two nerve trunks. The position of these organs probably reflects the initial stage of coelom's evolution.

Chlorite in the tube cavities typically occurs in the tube walls and forms relatively dark-colored and cryptocrystalline aggregates (Fig. 5d, e). The tube cavities are unevenly filled with hematite, quartz, chlorite, and leucoxene with rare inclusions of ankerite, apatite, and illite. Chlorite is locally replaced by finely dispersed hematite–quartz aggregates or quartz. The tubes often consist of segments, which served as the substrate for the precipitation of leucoxene (Fig. 5f); the latter is also concentrated in the cement of gossanites close to the tubes (Fig. 5d). Previous work has described fine rutile crystals associated with round apatite grains (60 μm in size) from the gossanites (Ayupova et al., 2016).

The Fe–Mg chlorite from the tube cavities belongs to the chamosite series with a ($FeO + Fe_2O_3$)/MgO ratio of >2.2 (Deer et al., 1962). The chlorite is characterized by the high content of $FeO + Fe_2O_3$ (38.58–46.42 wt.%) (Fig. 6a) and TiO_2 (0.23–0.50 wt.%), and Na_2O free relative to chlorite from chloritized hyaloclasts (25.36–29.63, 0.05–0.12, and 0.32–0.54 wt.%, respectively) (Table 2). Contents of Al_2O_3

Table 1
Chemical composition of hematite of tube microfossils, wt.%.

Fe_2O_3	Al_2O_3	SiO_2	CaO	MnO	MgO	P_2O_5	Total
Talgan deposit							
95.64	0.71	2.27	1.06	0.31	–	–	99.99
95.21	1.11	1.65	0.99	0.16	0.88	–	100.00
96.21	0.45	1.09	1.70	0.55	–	–	100.00
98.50	0.57	0.60	0.33	–	–	–	100.00
96.89	0.65	1.44	0.63	–	–	0.39	100.00
95.62	0.45	2.13	1.11	–	0.11	0.56	99.98
Priorskoye deposit							
96.35	0.94	1.20	1.52	–	–	–	100.10
97.88	0.63	0.35	1.14	–	–	–	100.00
94.98	1.51	2.42	0.42	–	0.68	–	99.01
Uchaly deposit							
95.00	1.39	2.78	0.26	–	0.57	–	100.00
97.41	0.37	1.86	0.36	–	–	–	100.00

Note. Dash – not determined.

(14.17–17.90 wt.%) and MgO (9.63–12.78 wt.%) are much lower in comparison to chlorite from hyaloclastites (20.02–21.07 and 13.06–14.35 wt.%, respectively). MnO is present in chlorite from both tube microfossils (0.79–1.34 wt.%) and hyaloclastites (1.21–1.44 wt.%)(Table 2). Distinct features of chlorite from tube microfossils are: (i) elevated total iron contents ($Fe/(Fe + Mg) = 0.64–0.71$) and (ii) elevated Fe^{3+} contents relative to Fe^{2+}($Fe^{3+}/(Fe^{3+}+Fe^{2+}) = 0.37–0.41$) compared with chlorite from the hyaloclasts (0.04–0.11 and 0.52–0.55, respectively) (Table 2). Chlorite from tube microfossils is enriched in Al in tetrahedral coordination (Al^{IV}/Al^{VI} 0.05–0.39), as compared with chlorite from hyaloclastites (Al^{IV}/Al^{VI} 0.91–1.08) (Fig. 6b).The Al^{IV} increases with increasing Fe^{3+}/Fe^{2+} and $Fe/(Fe + Mg)$ ratios (Table 2). The calculated temperatures of formation of chlorite from tube microfossils and hyaloclasts on the basis of chlorite geothermometer (Kranidiotis and Maclean, 1987) are 310–343 and 232–258 °C, respectively (Table 2).

Weaved fine tubular filaments 3–5 μm across and >300 μm long are constantly associated with hematite–chlorite tubes. These filaments are composed of spheres and are coated by a fine transparent cover, probably glycocalyx (Fig. 5g). Traces of burrowing or relics of glycocalix (locally, bacteria-free) are also easily identified as relict bacterial colonies or the hyphae of fungi (Fig. 5h). Stromatolite-like chlorite was found in association with tubes. Mineralized bacterial forms locally occur around hyaloclasts. This type of tube microfossils is abundant in the hematite–chlorite gossanites, which occur at the flanks of VHMS deposits containing abundant hyaloclastic material (Molodezhnoye, Alexandrinskoye, Babaryk, Sibai).

4.1.3. Carbonate–hematite tube microfossils

Carbonate–hematite tube microfossils (up to 300 μm across and 2–3 mm long) occur in gossanites enriched in carbonate material. Their structure also includes the wall and the cavity, with carbonates present in both. If the tubes are mostly composed of carbonates, they are characterized by concentric zoning (Fig. 7a-b). In some longitudinal sections, the tube microfossils exhibit a conical shape. Tubes are characterized by a fine (10 μm thick) hematite wall and a cavity made up of relatively dark carbonate or hematite (Fig. 7a, c). The wall of some tubes may be broken due to the fossilization process. Stromatolite-like leucoxene or hematite–carbonate aggregates were also found in association with tubes (Fig. 7d, g). The tubes composed of ankerite host randomly oriented filaments or fossilized mucus of the same composition (Fig. 7e and f). Single filaments composed of individual cells are typically smaller than 100 nm across (Fig. 7h) and similar to magnetotactic bacteria (Kopp and Kirschvink, 2008).

Mg-free calcite is a major mineral of these tube microfossils and is characterized by high MnO (1.99–4.26 wt.%) content (Table 3). Calcite also forms numerous rhombic crystals in the matrix of gossanites from the Talgan, XIX Parts'ezd, Novo-Shemur and Molodezhnoye VHMS deposits, locally up to 20% by volume. Ankerite is also often present in the tube cavities. Its chemical composition is rather stable (wt.%): CaO 26.51–28.00, FeO 18.70–23.75, MgO 6.99–8.91, and MnO 0.23–1.07 (Table 3). In gossanites of the Babaryk deposit, the tube microfossils are composed of monheimite (wt.%): ZnO 23.58–32.05, FeO 17.53–23.83, MnO 11.44–13.00, CaO 0.57–2.14 (Table 3). Siderite is associated with tube fragments from the Talgan deposit (containing MgO 3.48–5.75 wt.%, MnO 0.19–1.11 wt.%, and CaO 0.38–0.54 wt.%) (Table 3). At the Alexandrinskoye deposit, dolomite forms rhombic crystals in gossanite matrix, with up to 0.19 wt.% MnO and 0.22–1.63 wt.% FeO (Table 3).

The carbonate–hematite tube microfossils are abundant in the carbonate-rich gossanite layers. These also contain the hematite–quartz aggregates replacing the hyaloclasts (or rarely sulfide clasts), together with authigenic chalcopyrite, galena, crystalline pyrite and pyrite nodules. These microfossils have been found in the Talgan, XIX Parts'ezd, Alexandrinskoye, and Babaryk VHMS deposits.

4.2. Tomography of tube microfossils

Tomographic studies allowed us to specify the size and the structure of the tube microfossils from the Talgan, Molodezhnoye and Alexandrinskoye VHMS deposits. High-quality results were obtained for hematite (Talgan) and hematite–chlorite (Molodezhnoye) tubes. In 3D tomographic images, these tubes are well individualized relative to the host rock. The tubes are characterized by specific orientation, variable size, round transverse and tubular longitudinal sections, and well visible outer wall (Fig. 8, Appendix A). The largest specimens were found among hematite–chlorite tubes with a diameter of transverse section of up to 0.3 mm and a length of 6 mm (Fig. 8a, b). The tube walls demonstrate clear wavy microlayering from outer and inner sides, which may reflect segmentation of the tube worms (Fig. 8c, d).

4.3. Carbon and oxygen isotopes

The carbon and oxygen isotopic composition of authigenic Mn-bearing calcite and ankerite from the tube microfossils is shown in Table 4. Previously, it was found that carbon isotopic compositions range from −26.2 to −4.2‰ (Ayupova et al., 2015). New analyses of carbonates (−6.5, −9.0, −19.5‰) also fall to this range. The carbon isotopic composition of carbonates associated with the tube microfossils from hematite–quartz and hematite–carbonate gossanites is similar (av. −7.2 and − 6.8‰, respectively), whereas carbonates from hematite–chlorite gossanites are characterized by significantly lighter compositions (av. −22.8‰). The oxygen isotopic composition of carbonates associated with tube microfossils shows a range from +8.6 to +18.7‰ and is similar in all three types of rocks (av. +13.5, +14.2, +13.0‰).

For comparison, we also analyzed the carbon and oxygen isotopic composition of carbonates from crinoid-bearing carbonate clasts and calcite from hanging-wall limestones of the studied VHMS deposits (Table 4). Crinoid-bearing carbonate clasts are characterized by a narrow range of $\delta^{13}C$ values varying from −0.64 up to +2.20‰, with an average value of +0.93‰, similar to those of carbonates from limestones (−0.50 to +2.31‰, av. +0.84‰) and marine carbonates (Hoefs, 1997). The $\delta^{13}O$ values of crinoid-bearing carbonate clasts and carbonate from limestone are similar and range from +17.5 to +20.0‰. The $\delta^{18}O$ and $\delta^{13}C$ values of carbonates from hematite–quartz and hematite–carbonate gossanites are comparable with those of carbonates from wall of pyritized vestimentiferans found in massive sulfide ores of the Sibai deposit (Table 4).

The $\delta^{18}O$ and $\delta^{13}C$ values of carbonates from hematite–quartz and hematite–carbonate gossanites show insignificant correlation coefficient (0.48) for nine samples, whereas those of carbonates from hematite–chlorite gossanites exhibit no correlation (Fig. 9). According

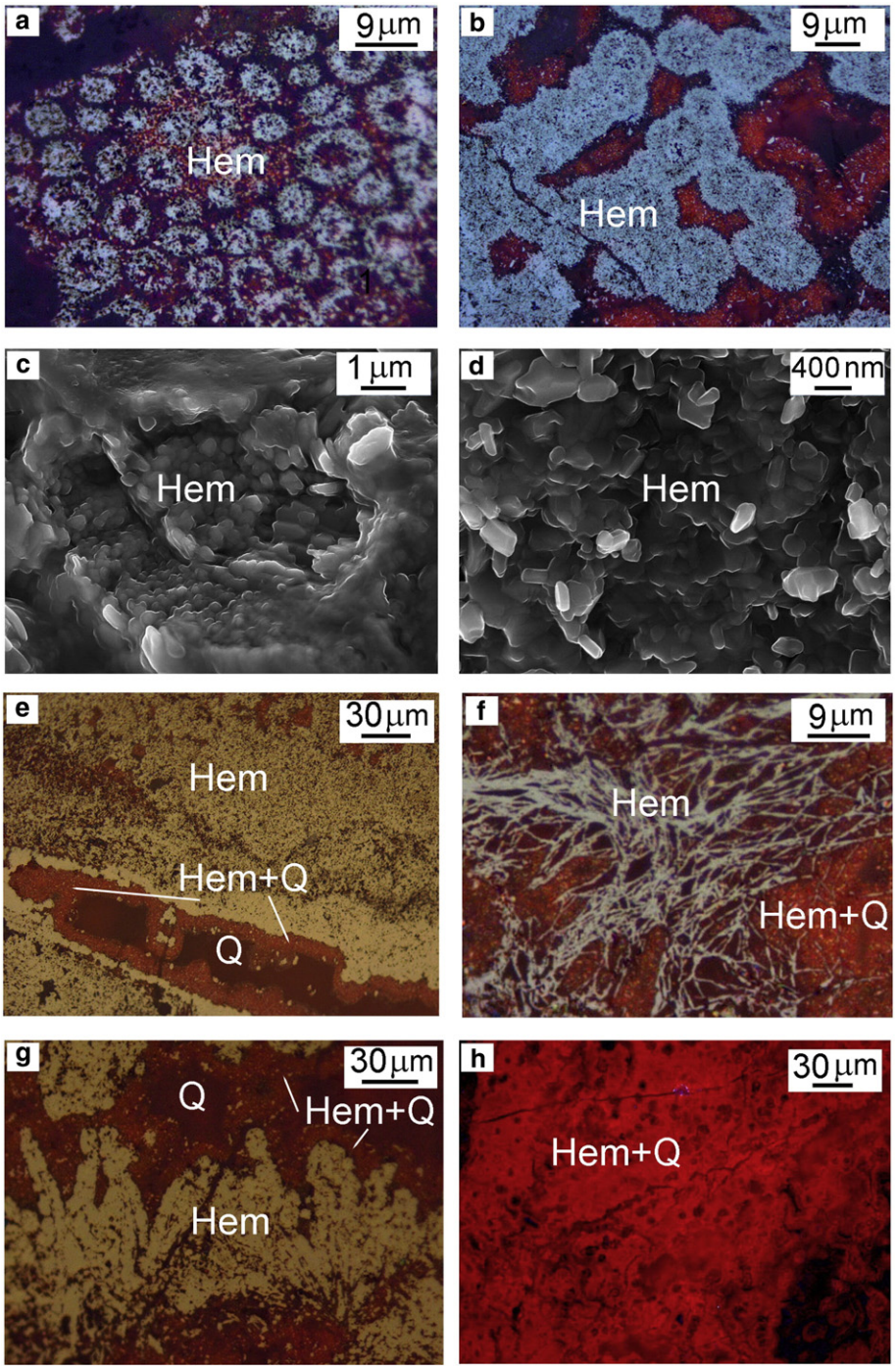

Fig. 4. Spherical and filamentous textures of hematite tube microfossils: a – zonal spheres in cavity, b – radial aggregates of fine hematite crystals inside the spheres; c – the inner structure of the sphere composed of hematite nanocrystals; d – fine-scaly hematite nanocrystals (detail of Fig. 4c); e – microstromatolite structure of hematite on the tube surface; f – randomly or unidirectionally oriented filaments in stromatolites; g – radial cellular hematite filaments (probably, fungi); h – traces of burrowing or relict glycocalix. Talgan deposit.

to Kim and O'Neil (1997), the calculated temperatures of formation of carbonates based on a 0‰ fluid vary from 70 to 166 °C.

4.4. Trace elements in hematite of tube microfossils

The LA–ICP–MS analysis shows a relatively uniform and stable distribution of trace elements in hematite from the tube microfossils (Table 5, Fig. 10a). Hematite from the Talgan deposit is characterized by the high contents of the following rock-forming elements (average): Si (8036 ppm), Al (2762 ppm), Mg (962 ppm), Ca (8791 ppm) (Ayupova et al., 2016). Enrichment of hematite in these rock-forming elements is also typical of the Alexandrinskoye deposit. The LA–ICP–MS trends indicate the presence of microinclusions of quartz, chlorite, and carbonate in hematite (Fig. 10b), which have been confirmed under the microscope. In spite of the low Ti contents in hematite (average 148 ppm), the LA–ICP–MS trend of Ti is uneven and is characterized by sharp amplitudes that are probably related to the presence of leucoxene microinclusions.

Hematite of the tube microfossils from the Talgan deposit is characterized by the high contents (maximum) of Mn (9393 ppm), As (1873 ppm), V (780 ppm), W (1091 ppm), Mo (34 ppm), and U (9 ppm) (Ayupova et al., 2016). Finely dispersed hematite–quartz

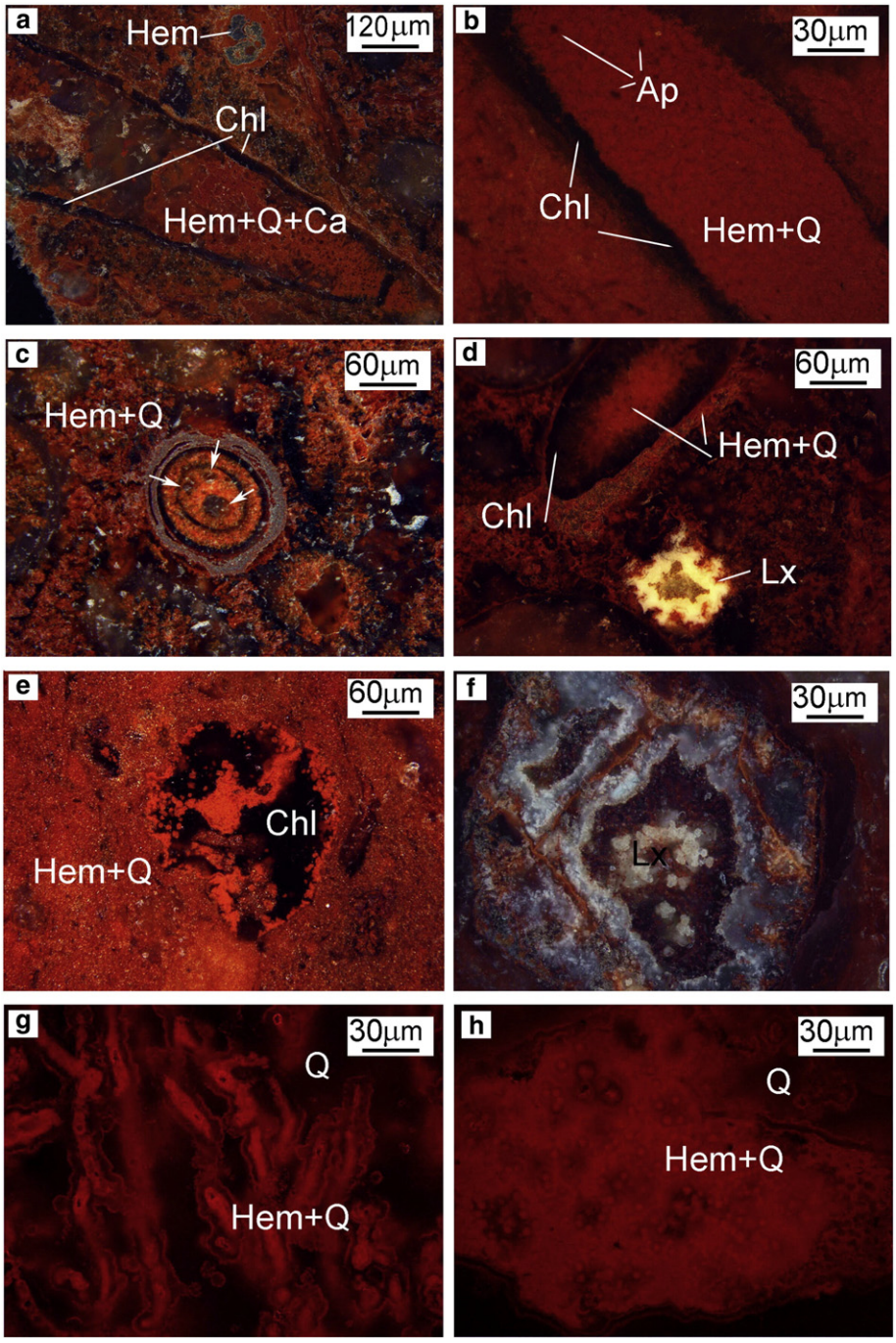

Fig. 5. Hematite–chlorite tube microfossils: a – hematite–chlorite wall and hematite–quartz and quartz cavity (longitudinal section); b – fine microlayers of hematite and chlorite of the wall and granular hematite–quartz aggregates with numerous inclusions of apatite and illite in the cavity; c – well-preserved inner structure of the tubes: coelom and mineralized organs of digestive and nerve systems; d – zonal distribution of chlorite and hematite–quartz aggregates in the cavity and leucoxene (white) in cement; e – interrelation between hematite–quartz material and chlorite (black) in the cavity and finely dispersed hematite wall; f – segmentation of the cavity emphasized by leucoxene aggregates; g – tubular filaments coated by fine transparent cover; h – relict glycocalyx. Chl – chlorite, Hem + Q + Ca –hematite + quartz + Mn-bearing calcite, Hem – hematite, Hem + Q – hematite–quartz aggregates, Lx – leucoxene. Dark field images. Molodezhnoye (a, c, f, g, h), Alexandrinskoye (b, d) and Babaryk (e) deposits.

aggregates of the tube microfossils of the Alexandrinskoye deposit are characterized by the lowest contains of these elements (maximum): Mn (1094 ppm), As (210 ppm), V (613 ppm), W (526 ppm). The flat LA–ICP–MS trends of these elements (Fig. 10c) indicate their incorporation into the structure of hematite. Trace element composition of hematite from the tube microfossils and hematite of ambient bacterial textures is similar.

In this study, for comparison we also analyzed trace elements compositions of the following minerals: (i) pseudomorphic hematite after sulfide clasts, (ii) late chalcopyrite filling the cavities of some tube microfossils, (iii) chlorite from hyaloclasts of gossanites, (iv) framboidal and (v) crystalline pyrite from tube microfossils of sulfide ores (Table 5). The high content of sulfide-associated trace elements (Cu, Zn, Pb, Sb, Te, Se) in pseudomorphic hematite is several times higher than that of hematite from tube microfossils (Fig. 11). Direct correlation between Pb and Sb contents is typical for all studied samples (Fig. 12a). The contents of V, W, Mo, Uand As are rather stable and are similar in both pseudomorphic hematite and hematite of the tube microfossils (Table 5, Figs. 11 and 12b-d). The Ti and Mn contents in pseudomorphic hematite are highly variable (Table 5). Late chalcopyrite from the tube

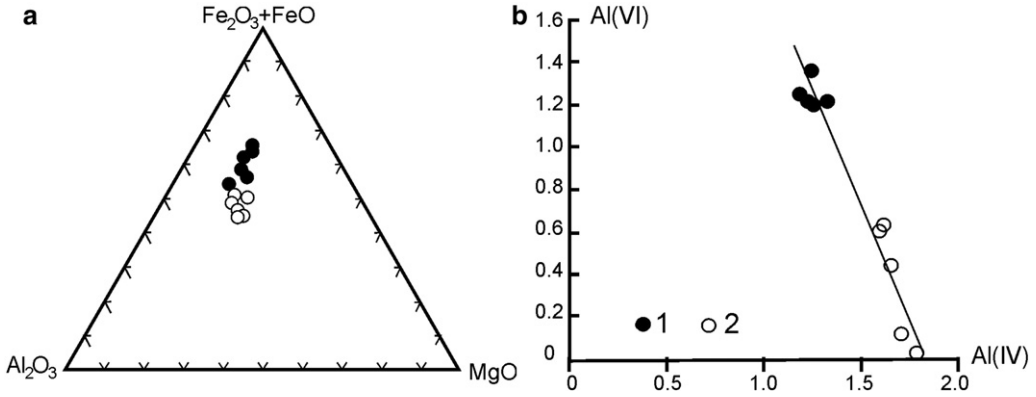

Fig. 6. (a) Ternary Al_2O_3–Fe_2O_3 + FeO–MgO with compositions of chlorite from tube microfossils (filled circle, 1) and hyaloclasts (open circle, 2) and (b) distribution of aluminium in tetrahedral (Al^{VI}) versus octahedral (Al^{IV}) sites; the legend is the same as in (a). 1 – tube microfossils (Molodezhnoye and Alexandrinskoye deposits); 2 – hyaloclasts (Molodezhnoye and Uzelga deposits).

microfossils and chlorite from hyaloclasts are enriched only in Mn and V, whereas pyritized fossils from the sulfide ores are characterized by the high Mn, As, and Mo contents (Table 5). Both framboidal and crystalline pyrite of tube microfossils in sulfide ores is characterized by high contents of Mn, Cu, Zn, Pb, Sb, As and Tl (Table 5).

5. Discussion

5.1. Comparison with sulfidized tube fossils in sulfide ores

A rich fossil vent fauna, which includes vestimentiferans and polychaetes, has been identified in a number of the Uralian VHMS deposits

Table 2
Chemical composition of chlorite of tube fossils (1–5) and chloritized hyaloclasts (6–10), wt.%.

	SiO_2	TiO_2	Al_2O_3	FeO	MgO	MnO	CaO	Na_2O	Total
Tube microfossils									
Molodezhnoye deposit									
1	21.39	0.50	14.52	45.58	10.59	0.79	0.29	–	93.66
2	21.47	0.37	16.41	42.39	9.63	1.25	–	–	91.52
3	23.03	0.23	17.87	38.58	12.38	1.18	–	–	93.27
Alexandrinskoye deposit									
4	22.31	0.27	17.90	39.94	10.40	1.34	–	–	92.16
5	20.56	0.38	14.17	46.42	10.50	0.99	–	–	93.02
Hyaloclasts									
Molodezhnoye deposit									
6	26.88	0.07	20.40	28.10	14.35	1.44	–	0.54	94.49
7	26.95	0.05	20.12	28.22	14.07	1.28	–	0.52	94.19
8	27.36	0.06	20.15	27.82	13.98	1.19	0.16	0.55	94.50
Uzelga deposit									
9	26.18	0.10	21.07	29.63	13.31	1.44	0.13	0.49	93.94
10	24.98	0.12	20.02	25.36	13.06	1.21	0.16	0.32	88.37

	Si	Ti	Al^{IV}	Al^{VI}	Fe^{2+}	Fe^{3+}	Mg	Ca	Mn	Na	Fe^{3+}/Fe^{2+}	Fe/(Fe + Mg)	*T°C
1	2.28	0.04	1.72	0.12	2.53	1.53	1.69	0.03	0.07	—	0.60	0.71	329
2	2.34	0.03	1.66	0.44	2.70	1.16	1.55	—	0.12	—	0.42	0.71	318
3	2.40	0.02	1.60	0.60	2.40	0.96	1.92	—	0.10	—	0.40	0.64	310
4	2.38	0.02	1.62	0.63	2.62	0.95	1.66	—	0.12	—	0.36	0.68	310
5	2.21	0.03	1.79	0.01	2.46	1.72	1.69	—	0.09	—	0.70	0.71	343
6	2.74	0.01	1.26	1.19	2.24	0.16	2.18	—	0.11	0.11	0.07	0.52	246
7	2.77	0.01	1.23	1.21	2.32	0.10	2.15	—	0.11	0.10	0.04	0.53	240
8	2.81	0.01	1.19	1.24	2.34	0.10	2.14	0.02	0.10	0.11	0.04	0.53	232
9	2.67	0.01	1.33	1.21	2.32	0.20	2.03	0.01	0.12	0.10	0.09	0.55	258
10	2.75	0.01	1.25	1.35	2.04	0.26	2.14	0.02	0.11	0.07	0.12	0.52	246

Crystal chemical formula.
1) $[(Fe^{2+}_{1.25}Fe^{3+}_{0.66}Mn_{0.07}Ti_{0.04})_2(Fe^{3+}_{0.89}Al_{0.11})(Si_{2.28}Al_{1.72})_4O_{10}(OH)_2](Mg_{1.69}Fe^{2+}_{1.28}Ca_{0.03})_3(OH)_6$.
2) $[(Fe^{2+}_{1.25}Fe^{3+}_{0.60}Mn_{0.12}Ti_{0.03})_2(Fe^{3+}_{0.56}Al_{0.44})(Si_{2.34}Al_{1.66})_4O_{10}(OH)_2](Mg_{1.55}Fe^{2+}_{1.45})_3(OH)_6$.
3) $[(Fe^{2+}_{1.32}Fe^{3+}_{0.56}Mn_{0.10}Ti_{0.02})_2(Fe^{3+}_{0.40}Al_{0.60})(Si_{2.40}Al_{1.60})_4O_{10}(OH)_2](Mg_{1.92}Fe^{2+}_{1.08}Ca_{0.03})_3(OH)_6$.
4) $[(Fe^{2+}_{1.28}Fe^{3+}_{0.58}Mn_{0.12}Ti_{0.02})_2(Fe^{3+}_{0.37}Al_{0.63})(Si_{2.38}Al_{1.62})_4O_{10}(OH)_2](Mg_{1.66}Fe^{2+}_{1.34}Ca_{0.03})_3(OH)_6$.
5) $[(Fe^{2+}_{1.15}Fe^{3+}_{0.73}Mn_{0.09}Ti_{0.03})_2(Fe^{3+}_{0.99}Al_{0.01})(Si_{2.21}Al_{1.79})_4O_{10}(OH)_2](Mg_{1.69}Fe^{2+}_{1.31}Ca_{0.03})_3(OH)_6$.
6) $[(Fe^{2+}_{1.53}Al_{0.19}Fe^{3+}_{0.16}Mn_{0.11}Ti_{0.01})_2Al(Si_{2.74}Al_{1.26})_4O_{10}(OH)_2](Mg_{2.18}Fe^{2+}_{0.71}Na_{0.11})_3(OH)_6$.
7) $[(Fe^{2+}_{1.57}Al_{0.21}Fe^{3+}_{0.11}\ Mn_{0.11}Ti_{0.01})_2Al(Si_{2.77}Al_{1.23})_4O_{10}(OH)_2](Mg_{2.15}Fe^{2+}_{0.75}Na_{0.10})_3(OH)_6$.
8) $[(Fe^{2+}_{1.61}Al_{0.24}Fe^{3+}_{0.04}Mn_{0.10}Ti_{0.01})_2Al(Si_{2.81}Al_{1.19})_4O_{10}(OH)_2](Mg_{2.14}Fe^{2+}_{0.73}Na_{0.11}Ca_{0.02})_3(OH)_6$.
9) $[(Fe^{2+}_{1.67}Al_{0.24}Fe^{3+}_{0.20}Mn_{0.12}Ti_{0.01})_2Al(Si_{2.67}Al_{1.33})_4O_{10}(OH)_2](Mg_{2.03}Fe^{2+}_{0.65}Na_{0.10}Ca_{0.01})_3(OH)_6$.
10) $[(Fe^{2+}_{1.62}Al_{0.35}Fe^{3+}_{0.26}Mn_{0.10}Ti_{0.01})_2Al(Si_{2.75}Al_{1.25})_4O_{10}(OH)_2](Mg_{2.14}Fe^{2+}_{0.42}Na_{0.07}Ca_{0.02})_3(OH)_6$.
Note. Dash – not determined. Structural formula are calculated from chemical composition $(Mg,Fe)_3(Si,Al)_4O_{10}(OH)_2 \cdot 3(Mg,Fe)(OH)_6$, assuming 14 oxygen atoms. Chlorite compositional geothermometry (T °C) is based on the number of ions of tetrahedral Al and Fe/(Fe + Mg) values (Kranidiotis and Maclean, 1987): $T\,°C = 106A1^{IV}_{cor} + 18$, a correction for increase in $A1^{IV}$ with Fe/(Fe + Mg) must be made: $Al^{IV}_{corrected} = Al^{IV}_{sample} - 0.7 \times Fe/(Fe + Mg)$.

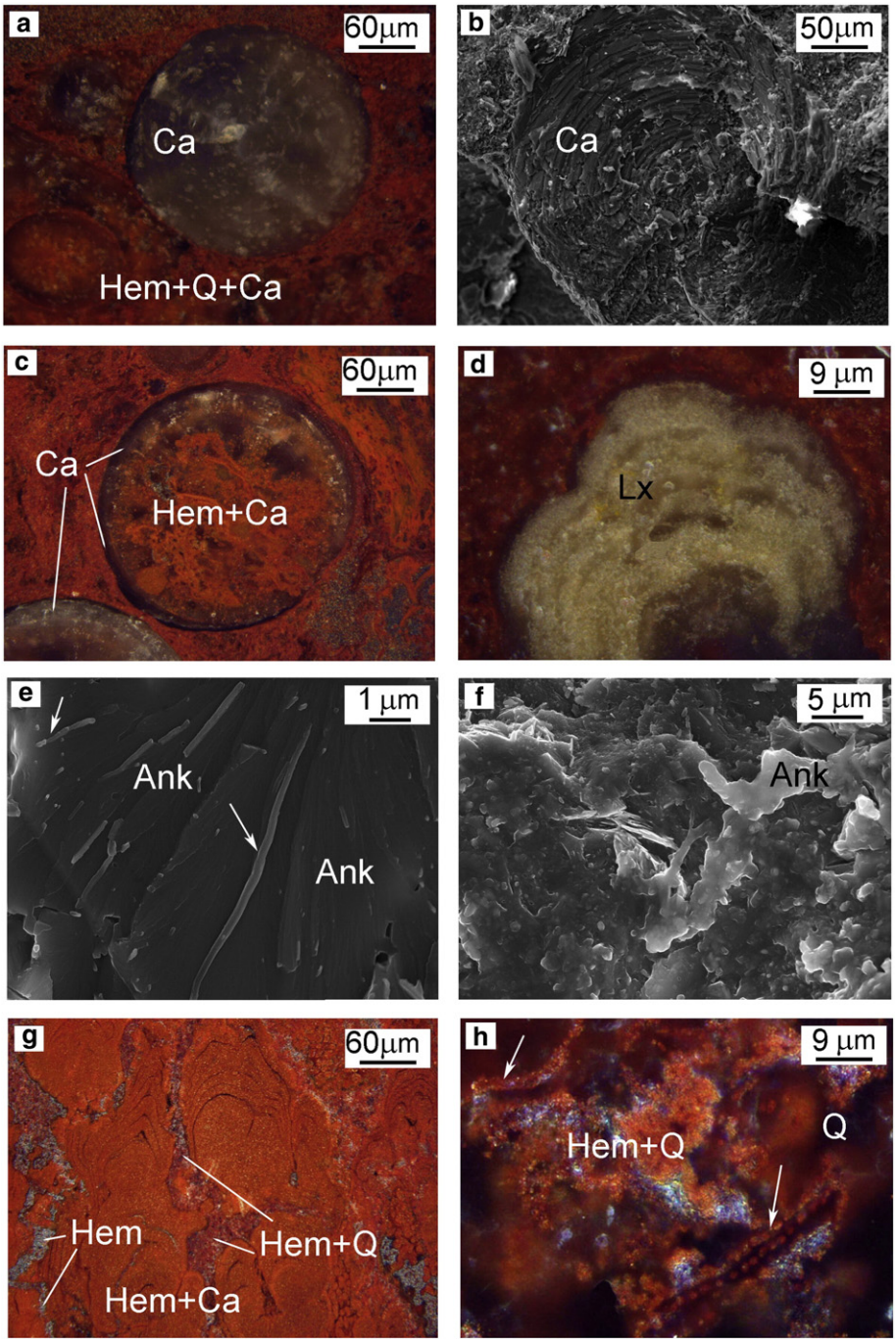

Fig. 7. Carbonate–hematite tube microfossils: a – fine tube wall composed of finely dispersed hematite and cavity composed of Mn-bearing calcite; b – concentric–zonal structure of Mn-bearing calcite within the tube; c – hematite–carbonate tubes; d – stromatolitic leucoxene aggregates; e – ankerite filaments within ankerite tubes; f – ankerite glycocalyx within tubes; g – hematite–carbonate stromatolites in matrix of gossanites; h – cellular structure of single filaments. Ca – Mn-bearing calcite, Hem + Ca – hematite–Mn-bearing calcite aggregates, Lx – leucoxene, Ank – ankerite, Hem + Q – hematite–quartz aggregates. Dark field images (a, c, d, d, h), SEM-photo (b, e, f). Samples come from the gossanite horizons of the Talgan (a, b, d, e, g, h) and XIX Parts'ezd (c, f) deposits.

(Little et al., 1999; Maslennikov, 2006; Zaykov, 2006; Maslennikov et al., in press) – similar to that of the oxygen-depleted vent systems of the modern ocean (e.g., Juniper et al., 1992; Demina et al., 2007). Pyritized polychaete colonies dominate in the sulfide ores. Tube microfossil worms were found in clastic ores from the Talgan, Novo–Shemur, Blyava, and Priorskoye VHMS deposits, where they are overlapped by gossanites (Fig. 13a,b). The microfossils with a variable diameter (100–200 μm, up to 5 mm) are characterized by a microlayered wall. The outer part of the walls are composed of crystalline pyrite with a relict colloform–laminar structure, and their inner parts encrusted by crystalline pyrite. Quartz layers probably replace organic layers, and may be observed between the pyrite layers. The interior of the tubes is filled with As-bearing pyrite (up to 5663 ppm As). Chalcopyrite of the interior filling replaces framboidal pyrite. Diverse bacterial morphotypes were reported on the interior and exterior surfaces of the tubes (Maslennikov, 2006).

The morphology, size, and internal structure of the hematitized tubes from gossanites are comparable with those of sulfidized polychaetes from the sulfide ores described above. Similar structures are also typical of rare tubes with hematite–quartz microlayered walls

Table 3
Chemical composition of carbonates, wt.%.

CaO	MnO	FeO	MgO	ZnO	Crystal chemical formula
Mn-bearing calcite					
XIX Parts'ezd deposit					
53.60	2.01	–	–	–	$(Ca_{0.97}Mn_{0.03})_{1.00}(CO_3)_{1.00}$
53.65	1.99	0.44	–	–	$(Ca_{0.96}Mn_{0.03}Fe_{0.01})_{1.00}(CO_3)_{1.00}$
53.40	2.08	–	–	–	$(Ca_{0.97}Mn_{0.03})_{1.00}(CO_3)_{1.00}$
50.98	4.26	0.58	–	–	$(Ca_{0.93}Mn_{0.06}Fe_{0.01})_{1.00}(CO_3)_{1.00}$
Talgan deposit					
52.38	2.82	0.53	–	–	$(Ca_{0.95}Mn_{0.04}Fe_{0.01})_{1.00}(CO_3)_{1.00}$
51.73	3.18	0.68	–	–	$(Ca_{0.94}Mn_{0.05}Fe_{0.01})_{1.00}(CO_3)_{1.00}$
52.06	3.67	0.06	–	–	$(Ca_{0.95}Mn_{0.05})_{1.00}(CO_3)_{1.00}$
52.03	2.09	1.48	–	–	$(Ca_{0.95}Mn_{0.03}Fe_{0.02})_{1.00}(CO_3)_{1.00}$
Ankerite					
Molodezhnoye deposit					
28.00	0.59	18.70	6.99	–	$(Ca_{1.00}Fe_{0.58}Mg_{0.40}Mn_{0.02})_{2.00}(CO_3)_{2.00}$
26.69	0.34	23.75	6.84	–	$(Ca_{0.98}Fe_{0.68}Mg_{0.34})_{1.00}(CO_3)_{2.00}$
26.78	0.23	23.27	7.41	–	$(Ca_{0.96}Fe_{0.66}Mg_{0.38})_{2.00}(CO_3)_{2.00}$
Talgan deposit					
26.51	1.07	20.36	7.98	–	$(Ca_{0.98}Fe_{0.58}Mg_{0.40}Mn_{0.04})_{2.00}(CO_3)_{2.00}$
27.03	0.95	21.02	8.91	–	$(Ca_{0.96}Fe_{0.58}Mg_{0.44}Mn_{0.02})_{2.00}(CO_3)_{2.00}$
26.96	0.44	23.30	6.91	–	$(Ca_{0.98}Fe_{0.66}Mg_{0.34}Mn_{0.02})_{2.00}(CO_3)_{2.00}$
Monheimite					
Babaryk deposit					
0.57	12.00	17.53	–	32.05	$(Zn_{0.48}Fe_{0.30}Mn_{0.21}Ca_{0.01})_{1.00}(CO_3)_{1.00}$
1.17	11.58	23.46	–	26.08	$(Zn_{0.39}Fe_{0.39}Mn_{0.20}Ca_{0.02})_{1.00}(CO_3)_{1.00}$
1.24	11.44	22.32	–	26.87	$(Zn_{0.40}Fe_{0.38}Mn_{0.20}Ca_{0.02})_{1.00}(CO_3)_{1.00}$
1.85	12.53	23.83	–	23.58	$(Zn_{0.35}Fe_{0.40}Mn_{0.21}Ca_{0.04})_{1.00}(CO_3)_{1.00}$
1.90	13.00	22.31	–	24.85	$(Zn_{0.37}Fe_{0.37}Mn_{0.22}Ca_{0.04})_{1.00}(CO_3)_{1.00}$
2.14	12.98	23.48	–	24.04	$(Zn_{0.35}Fe_{0.39}Mn_{0.22}Ca_{0.04})_{1.00}(CO_3)_{1.00}$
Siderite					
Talgan deposit					
0.54	0.19	55.52	5.75	–	$(Fe_{0.84}Mg_{0.15}Ca_{0.01})_{1.00}(CO_3)_{1.00}$
0.38	0.43	57.70	3.48	–	$(Fe_{0.89}Mg_{0.09}Mn_{0.01}Ca_{0.01})_{1.00}(CO_3)_{1.00}$
0.40	1.11	56.34	4.11	–	$(Fe_{0.87}Mg_{0.11}Mn_{0.01}Ca_{0.01})_{1.00}(CO_3)_{1.00}$
Dolomite					
Alexandrinskoye deposit					
31.27	–	0.22	21.12	–	$(Ca_{1.02}Mg_{0.96}Fe_{0.02})_{2.00}(CO_3)_{2.00}$
29.92	0.19	1.63	21.05	–	$(Ca_{1.00}Mg_{0.96}Fe_{0.04}Mn_{0.001})_{2.00}(CO_3)_{2.00}$

Note. Dash – not determined. Number of cations on the basis of $Ca^{2+} + Mg^{2+} + Fe^{2+} + Mn^{2+} = 1$ (calcite, monheimite and siderite) or 2 (dolomite, ankerite).

and chalcopyrite fills (Fig. 13c). Both the sulfidized polychaetes (from the sulfide ores) and the hematitized tubes (from gossanites) probably belong to the phylum Annelida.

The orientation of the hematite (hematite–quartz) tube colonies and rare segmentation of their former bodies (Fig. 3) may be a feature of very small siboglinids (vestimentiferans?), which were fossilized in their life positions. Spherical forms saturated with Fe-oxidizing bacteria inside the tubes (Fig. 4a-d) are probably the analogs of trophosomes (Felbeck, 1981). The fossil tubes show the ubiquitous presence of filamentous and stromatolic bacteria or fungi (Fig. 4e-h). The transition between sulfide-rich anoxic sediments and oxygenated bottom waters was favourable for the oxidation of sulfides and preservation of the tube worms.

The disordered aggregates of the hematite–chlorite tubes, the structural peculiarities of their mineralized soft tissues (Fig. 5), and segmentation of their former bodies (Figs. 5a, 8) allow their comparison with polychaetes. Abundant filamentous bacteria are associated with hematite–chlorite tubes: some microbial communities are present on the surface of the tubes, while others are found in the matrix of gossanites (Fig. 5g, h), similar in many respects to the fossilized polychaetes from the sulfide ores (Maslennikov, 2006). It is considered that bacteria, which are present on the tube surfaces, have autotrophic metabolisms and synthesize organic matter from the mineral carbon (Berg et al., 2010). Intercalated hematite and chlorite microlayers in the tube walls resemble microlayers of pyrite and quartz in the walls of sulfidized polychaets. The fossilization of well-preserved soft tissue in the tubes, well-preserved filaments coated by a fine transparent cover, and the presence of probable glycocalyx, indicate alteration of primary sediments during early diagenesis. Most likely, the abundance of hyaloclastic material in the primary sediments was responsible for the mineral composition of the tube fossils.

The similarity of the carbonate–hematite tube microfossils with calcareous serpulids is indicated by several lines of evidence: a similar morphology to magnetotacticum bacteria, their conical shape, the concentric–zonal structure of carbonates inside the tubes, abundant ankerite filaments, glycocalyx within the tubes, and stromatolic hematite–carbonates and leucoxene aggregates (Fig. 6) (Vinn and Mutvei, 2009). According to Frankel et al. (1983), the cells of magnetotacticum bacteria consist of Fe^{3+} oxy-hydroxide phases together with the magnetosomes. They precipitate Fe_3O_4 in the sequence: Fe^{3+} quinate → Fe^{2+} → low density hydrous ferric oxide → ferrihydrite → Fe_3O_4.

Thus, the biodiversity of tube worms and their mineral composition reflect the diverse primary substrates in different proportions (sulfides, hyaloclasts, carbonates) during the formation of the gossanites. Each type of tube microfossil is characterized by specific bacterial assemblages. The morphological and structural features of the tube microfossils, filaments, thin films and spherical bodies are strong evidence of their organic origin rather than the products of inorganic precipitation during the formation of the gossanites.

The well-preserved microfossils indicate diagenetic transformation of primary sediments. Post-burial processes leading to exceptional preservation are still largely unresolved, although oxygen-deficient conditions seem to be an important factor in their preservation (Allison, 1988), particularly where diagenetic mineralization is involved (Briggs

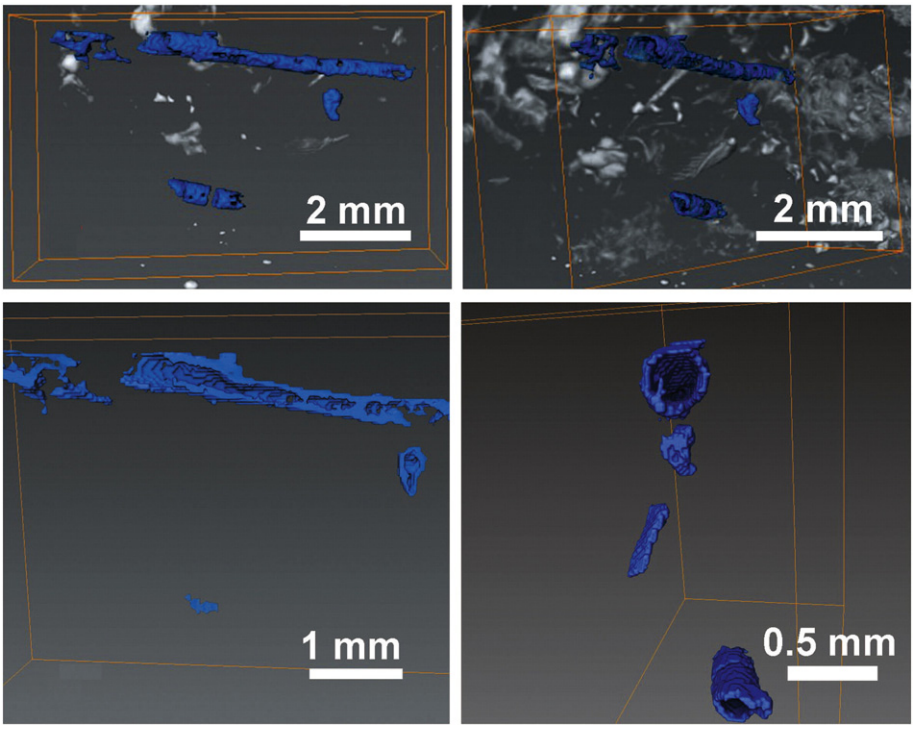

Fig. 8. 3D tomographic images of chlorite–hematite tube microfossils with visible wavy microlayering. Molodezhnoye deposit, sample Mol-9.

et al., 1996). Fe-oxides and Fe-aluminosilicates are dominant minerals responsible for the replicating of delicate tissues during diagenesis (Jin et al., 1991). Early diagenetic replication of non-mineralized tissue by minerals played an important role in the exceptional preservation of fossils (Zhu et al., 2001). Experimental studies suggest that iron minerals might also play a role in maintaining the structural and chemical integrity of fossils under diagenetic conditions (Picard et al., 2015).

The tubes worms may have utilized bacteria in a manner similar to those at modern hydrothermal vent sites. Bacterially mediated reactions not only represent an important link in the food chain that is developed in habitats, but also modify the pore fluid chemistry and influence the chemical processes in sediments. The microstromatolitic textures associated with the tube worms probably represents fungal colonies. The presence of iron or iron–silica oxide filamentous textures with a wide variety of morphologies is a peculiarity of Fe-oxide deposits from the modern and ancient ocean (Juniper and Fouquet, 1988; Hannington and Jonasson, 1992; Grenne and Slack, 2003; Little et al., 2004). Filamentous and coccoidal fossilized microorganisms in subseafloor basalts of modern oceans have been interpreted as fossilized fungal colonies (Ivarsson et al., 2012; Dekov et al., 2013). Preservation of bacteria is related to the rapid fossilization process, which occurred prior to the beginning of degradation of bacterial bodies.

5.2. Authigenic minerals

The major authigenic minerals of the tube microfossils (hematite, quartz, chlorite, carbonates, apatite, and leucoxene) are responsible for the fossilization of chitin and soft tissues of the tube worms, since these mineral aggregates often replicate their morphology. The exceptional preservation of soft tissues requires elevated rather than restricted microbial activity (Sagemann et al., 1999). The type of minerals depends mainly on the composition of the sediments (sulfides, hyaloclasts, carbonates) and the ambient conditions created by their decay. Bacterial decomposition of organic matter is generally assumed to play an important role in fossil diagenesis, controlling pH, Eh, and form of mineral paragenesis during fossilization (Allison, 1988).

5.2.1. Hematite

Iron in gossanites comes from two different sources: (i) oxidation of sulfides and (ii) remobilization from hyaloclasts (see Maslennikov et al., 2012). Under more oxidizing conditions, Fe precipitates as iron oxyhydroxides and is later transformed to hematite (Table 6). In most cases, this alteration is pseudomorphic and is easily identified in gossanites (Maslennikov et al., 2012).

It was suggested that bacteria may oxidize Fe^{2+}, producing energy, and precipitate the iron oxide around bacterial filaments (e.g., Alt, 1988; Hannington and Jonasson, 1992). The rate of bacterial oxidation of Fe^{2+} released from pyrite surfaces is up to one million times faster than the inorganic oxidation rate at low pH (Singer and Stumm, 1970). Sulfide oxidation can be associated, for example, with development of *Beggiatoa* or *Thioploca* bacterial mats (Himmler et al., 2011). It was established that the oxidation of Fe^{2+} and further precipitation of its insoluble oxides around bacterial cells may be a result of interaction of Fe ions with H_2O_2 (Dubinina, 1978), which is released during microbial activity. Sulfuric acid generated by sulfide dissolution accelerates the dissolution of ambient hyaloclasts, increasing porosity and providing access for microbial colonization.

Under more oxidizing conditions, the hyaloclasts are destroyed with the formation of nontronite and further release of Fe and Si (Maslennikov et al., 2012, Table 6). In some cases, the hematitized filaments surround hyaloclasts (Fig. 14a,b). We believe that a combination of low pH and a bacteria-rich micro-environment may radically accelerate dissolution of hyaloclasts. Under neutral pH and low oxygen concentrations, chemolithoautotrophic Fe(II) oxidation (e.g., by *Gallionella ferruginea*) does lead to the high rates of formation of iron minerals (e.g., Søgaard et al., 2000). The tubular and granular structures of the rims of hyaloclasts are comparable with those resulted from microbial alteration of the basaltic glass of the oceanic crust (Torsvik et al., 1998; Furnes et al., 2001). Experimental studies show that bacteria are able

Table 4
Carbon and oxygen isotopic composition of calcite from quartz–hematite rocks of the Urals VHMS deposits.

Samples	VHMS deposits	$\delta^{13}C$ ‰, PDB	$\delta^{18}O$ ‰, VSMOW
Mn-bearing calcite associated with tube microfossils			
Hematite–quartz gossanites			
T-10	Talgan	−6.1*	+12.8
T-10/3	–"–	−7.5*	+15.3
S-1	Sibai	−6.5	+14.4
Al-12	Alexandrinskoye	−8.6*	+10.1
average		*−7.2*	*+13.5*
Hematite–carbonate gossanites			
T-5076-139.3	Talgan	−5.8*	+14.8
T-5104	–"–	−4.2*	+16.7
XIX-6108-71.3	XIX Parts'ezd	−9.0	+12.2
XIX-4	–"–	−6.4*	+18.7
Al-3	Alexandrinskoye	−8.5*	+11.2
average		*−6.8*	*+14.2*
Hematite–chlorite gossanites			
T-08/4	Talgan	−26.2*	+14.9
Mol-08/9	Molodezhnoye	−23.5*	+8.6
Mol-8006	–"–	−19.5	+15.7
Al-08/3	Alexandrinskoye	−21.9*	+12.9
average		*−22.8*	*+13.0*
Crinoid-bearing carbonate clasts			
T-5156-178.9	Talgan	−0.64*	+17.9
T-08/3	–"–	+0.97*	+18.7
T-08/1	–"–	+1.21*	+18.3
Uz-1	Uzelga	+2.20	+20.0
average		*+0.93*	*+18.7*
Calcite from hanging wall limestones			
Talg-Limest-1	Talgan	+1.09*	+18.21
XIX-Limest-1	XIX Parts'ezd	+2.31	+18.51
Sib-Limest-1	Sibai (Maslennikov, 1999)	+2.00	+19.22
5987-73	–"–	−0.50	+16.30
5837	–"–	−0.70	+17.50
average		*+0.84*	*+17.95*
Pyritized vestimentiferans with calcite			
2072-01	Sibai (Maslennikov, 1999)	−4.6	+15.0
2072-02	–"–	−4.7	+14.4
150-2	Oktyabrskoye (Maslennikov, 1999)	−13.2	+12.6
average		*−7.5*	*+14.0*

Notes. Samples of Mn-bearing calcite associated with tube microfossils could contain insignificant amount of ankerite. *, data of (Ayupova et al., 2016).

to transform completely the basaltic glass and enrich it in Fe, Si, Mn, P and K (Ferris et al., 1986; Thorseth et al., 1995).

Under oxidizing conditions where ferriginous material is abundant, diagenesis of sediment leads to fossilization of tube worms by iron

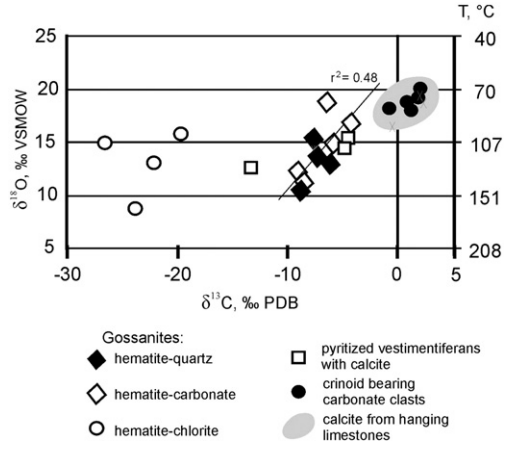

Fig. 9. Oxygen and carbon isotopic composition of carbonates from gossanites, pyritized vestimentiferans from sulfide ores (Maslennikov, 1999), and limestones. Temperatures are calculated by Kim and O'Neil (1997) using isotope equilibrium on-line calculator http://www.ggl.ulaval.ca/cgi-bin/isotope/generisotope.cgi.

oxyhydroxides (Table 6). Fine, scaly, and curved hematite from the outer wall indicates flexibility of the precursor material prior to mineralization. The presence of Al, Si, Ca, and locally, Mn, Mg and P in the hematite of the tube microfossils reflects the microinclusions of apatite, calcite and chlorite. Microbial mats have originally been encrusted by Fe (III) oxides and may thus represent Fe-oxidizing bacteria.

5.2.2. Chlorite

The replacement of the walls and interior of the tube microfossils by chlorite (chamosite) and iron oxides was probably caused by variable pH conditions, due to the presence of organic matter. Under a pH of >6 and higher, the ions of Al, Fe, and Si, are released during the destruction or dissolution of hyaloclasts, which could precipitate and further interact with Si ions leading to formation of amorphous smectite (Drennan, 1964). Reducing conditions, which should dominate in the polychaete environment, maintain Fe^{2+}. Further increase in pH (up to 9) results in a rapid increase in solubility of Al_2O_3 and SiO_2, and precipitation of Fe^{3+}. Any excess iron would react with organic matter and produce Fe-bearing carbonates (Drennan, 1964). Over time, after the complete fossilization of organic matter and slowdown of bacterial activity, redox conditions changed at the micro-level, and amorphous smectite was transformed to more stable chamosite, which replicated the structural peculiarities of dead tubes (Table 6).

Chamosite of the studied tube microfossils is characterized by high contents of the FeO + Fe_2O_3(38.58–46.42 wt.%), as well as a higher oxidation value and the absence of Na_2O (in comparison with chlorite of hyaloclasts; Table 2). The predominance of Fe^{3+} over Fe^{2+} in the chlorite of tube microfossils indicates relatively elevated alkaline conditions during the biomineralization processes. Decreased iron contents within chlorites constituting the hyaloclastites may indicate acid conditions due to the presence of sulfides. The role of acidity may be better assessed using the distribution of Al between octahedral and tetrahedral sites in chlorite: enrichment of Al in octahedral sites may be indicative of acid conditions, because the sum of bivalent cations in octahedral positions decreases with an unchanged Si/Al ratio in tetrahedral sites (Deer et al., 1962). The coexistence of these two types of chlorite suggest the assemblage was under equilibrium and may be a result of diffusion of matrix components during diagenesis. Chamosite and illite assemblages can be co-precipitated in sediments under a large range of values Eh (+0.5 to −0.6) and pH (from 5 to 9) conditions (Maynard, 1983).

Fe–Al silicate, assumed to be chamosite, is known to precipitate in the presence of bacteria (Ferris et al., 1987). Cell surfaces and associated polymers provide effective nucleation sites for secondary silicate mineral precipitation. The combination of a low pH and bacteria-rich microenvironment in the guts of annelid worms may radically accelerate mineral dissolution and precipitation of chamosite during digestion (Needham et al., 2004). Good preservation of filamentous bacteria associated with the tube microfossils in gossanites support the early diagenetic stage of primary sediments alteration.

The calculated temperatures of chlorite formation (cf., Kranidiotis and MacLean, 1987) are very high for the diagenetic processes (Table 2). In low-temperature conditions, the temperatures derived from empirical chlorite thermometers are distinct from those measured in situ and could significantly be overestimated: e.g., the measured temperature in sediments of the Gulf Coast area (southern Texas) is 216 °C vs. 380 ± 20 °C according to the geothermometer (Bourdelle, 2011). On the basis of empirical ratio between measured temperature from different geothermal systems and experimental d(001) value, the temperature of formation of finely-dispersed chlorite-berthierine assemblage after glauconite is 190 ± 20 °C, whereas that calculated after (Cathelineau, 1988) is 237 °C (Drits et al., 2001). The calculations for berthierine from the footwall stringer zone of the Archean Kidd Creek massive sulfide deposit, Ontario, based on the geothermometer of Kranidiotis and Maclean (1987) yield relatively high temperatures of ~350 °C (Slack et al., 1992). In this case, berthierine is characterized by

Table 5
Trace element composition of hematite, chalcopyrite and pyrite of the tube microfossils, and chlorite of hyaloclasts of the Urals VHMS deposits (LA–ICP–MS data, ppm).

	Fe	Cu	Zn	Pb	Sb	Se	Te	As	Mn	Ti	V	Mo	W	U	Tl
Hematite (±quartz) of tube microfossils (n 20)															
Talgan deposit															
1	690,000	0.47	254	281	222	1.96	0.20	1264	786	73	514	13.72	635	8.29	0.08
2	690,000	1.37	168	144	209	1.99	0.15	1595	460	84	639	20.76	994	5.22	0.14
3	690,000	0.93	113	166	258	1.46	0.27	770	394	114	780	33.81	828	6.55	0.07
4	680,000	0.32	192	125	190	2.00	0.81	1071	674	529	528	10.66	589	8.56	0.03
5	690,000	0.33	152	187	198	1.22	0.22	1873	502	144	647	33.57	1091	5.31	0.11
6	690,000	1.12	377	368	244	1.55	0.91	1543	776	151	557	30.30	800	8.63	0.03
7	650,000	4.14	675	541	278	1.39	0.69	1855	5545	132	425	26.92	607	7.98	0.02
8	640,000	1.39	146	104	159	1.20	0.05	636	9393	101	754	29.51	669	4.79	0.07
9	670,000	0.65	221	68	108	0.91	0.04	683	3272	101	676	14.84	601	3.78	0.10
10	680,000	24.44	98	1173	258	1.44	0.34	833	1417	66	588	13.82	619	8.68	0.11
11	660,000	0.31	45	64	124	1.82	0.26	1204	357	138	663	22.37	881	4.04	0.10
av	*675,455*	*3.22*	*221*	*293*	*204*	*1.54*	*0.36*	*1212*	*2143*	*148*	*616*	*22.75*	*756*	*6.53*	*0.08*
σ	*17,248*	*6.79*	*166*	*310*	*53*	*0.45*	*0.29*	*435*	*2756*	*123*	*101*	*8.17*	*167*	*1.87*	*0.04*
m	*680,000*	*0.93*	*167*	*166*	*209*	*1.46*	*0.31*	*1204*	*776*	*114*	*639*	*22.37*	*669*	*6.55*	*0.08*
Alexandrinskoye deposit															
12	700,000	0.10	41	103	11	7.64	0.86	195	641	29	521	69.73	242	11.67	0.01
13	700,000	0.50	44	116	14	3.05	0.28	137	861	33	420	69.48	340	2.63	0.06
14	700,000	2.45	38	134	15	0.85	1.16	139	1070	34	350	70.15	162	2.20	0.00
15	700,000	8.27	55	124	25	3.30	0.49	210	1094	56	540	43.96	250	1.48	0.00
16	700,000	0.84	33	134	13	2.32	0.33	111	995	83	349	69.37	466	2.23	0.01
17	700,000	0.92	39	77	7	0.52	0.00	60	604	162	244	85.19	234	1.91	0.00
18	700,000	5.18	35	43	11	3.68	0.71	61	432	16	478	7.41	527	2.77	0.01
19	700,000	1.80	24	12	1	3.15	0.79	20	898	16	511	10.23	100	0.40	0.01
20	700,000	2.38	12	6	1	1.94	0.48	17	403	35	613	21.05	109	0.48	0.00
av	*700,000*	*2.49*	*36*	*83*	*11*	*2.94*	*0.57*	*106*	*777*	*52*	*477*	*49.62*	*270*	*2.86*	*0.01*
σ	*700,000*	*2.65*	*12*	*51*	*7*	*2.08*	*0.35*	*71*	*265*	*46*	*116*	*29.70*	*149*	*3.41*	*0.02*
m	*700,000*	*1.80*	*38*	*103*	*11*	*3.05*	*0.49*	*111*	*861*	*34*	*478*	*69.37*	*242*	*2.20*	*0.01*
av	**686,500**	**2.90**	**138**	**198**	**117**	**2.17**	**0.45**	**714**	**1529**	**105**	**540**	**34.84**	**537**	**4.88**	**0.05**
Pseudomorphic hematite after sulfide clasts (n 17)															
Talgan deposit															
21	665,000	5.56	506	883	499	4.83	23.81	957	1769	6611	691	15.16	333	16.08	0.04
22	665,000	24.34	772	1813	835	6.26	4.85	1790	2989	8631	499	17.29	509	22.59	0.05
23	665,000	20.13	927	1727	1099	3.66	20.05	2376	3218	6422	403	16.96	277	9.93	0.04
24	690,000	0.79	287	127	303	0.37	0.12	928	8665	2283	162	118.50	955	4.91	0.02
25	570,000	10.66	1150	422	338	2.30	0.37	803	146,367	258	165	8.92	110	7.74	0.06
av	*651,000*	*12.30*	*728*	*994*	*615*	*3.48*	*9.82*	*1371*	*32,601*	*4841*	*384*	*35.37*	*437*	*12.25*	*0.04*
σ	*41,641*	*8.79*	*304*	*678*	*307*	*2.03*	*10.11*	*613*	*56,932*	*3084*	*202*	*41.68*	*289*	*6.34*	*0.01*
m	*665,000*	*10.66*	*771*	*883*	*499*	*3.66*	*4.85*	*957*	*3218*	*6422*	*403*	*16.96*	*333*	*9.93*	*0.04*
Alexandrinskoye deposit															
26	670,000	4.73	1099	377	51	14.24	0.34	72	19,731	2428	577	6.19	146	5.66	0.05
27	690,000	0.60	3954	82	65	5.37	0.35	65	1044	3191	719	13.73	120	12.01	0.10
28	660,000	1.26	1577	490	66	9.94	0.29	107	29,795	2256	618	16.02	173	7.92	0.17
29	670,000	1.10	521	309	56	12.79	2.08	75	20,143	1815	685	11.00	170	5.24	0.09
30	650,000	92.56	1467	3896	220	64.87	45.03	751	7314	16,189	553	19.24	408	11.45	0.08
31	650,000	7.56	658	3324	268	17.93	17.65	938	4426	12,215	331	30.67	377	8.30	0.25
32	580,000	1.27	8875	865	34	13.68	8.58	74	88,265	682	246	11.84	27	2.33	0.04
33	620,000	4.47	4462	783	51	17.80	23.93	97	67,152	1158	419	11.60	82	4.36	0.02
34	680,000	1.19	12,264	15	6	4.48	13.12	16	2787	165	303	0.73	5	5.11	0.05
35	700,000	1.17	975	58	69	1.55	0.77	84	300	2045	868	19.89	212	10.36	0.10
36	680,000	0.39	11,487	11	7	4.44	0.03	13	2615	193	430	0.77	21	1.02	0.02
37	670,000	15,160	5760	148	41	13.82	122.46	227	3402	2430	607	24.17	94	8.51	1.13
av	*660,000*	*1273*	*4425*	*863*	*78*	*15.07*	*19.55*	*210*	*20,581*	*3730*	*530*	*13.82*	*153*	*6.86*	*0.17*
σ	*31,358*	*4187*	*4107*	*1263*	*78*	*15.90*	*33.63*	*291*	*27,387*	*4837*	*179*	*8.56*	*124*	*3.34*	*0.30*
m	*670,000*	*2*	*2765*	*343*	*53*	*13.24*	*5.33*	*80*	*5870*	*2150*	*565*	*12.79*	*133*	*6.79*	*0.08*
av	**657,353**	**902**	**3338**	**901**	**236**	**11.67**	**16.69**	**551**	**24,116**	**4058**	**487**	**20.16**	**236**	**8.44**	**0.13**
Authigenic chalcopyrite from cavities of tube microfossils (n 10)															
Talgan deposit															
38	325,000	332,589	399	43	21	43.66	2.11	44	2176	52	64	0.41	9	0.06	1.65
39	325,000	328,991	13	152	12	6.54	1.50	31	213	2	7	0.05	59	0.00	0.12
40	320,000	322,404	20	5242	21	2.11	0.75	58	525	5	12	0.49	121	0.02	0.12
41	325,000	320,534	36	2227	12	4.92	3.05	35	349	5	6	0.49	22	0.01	0.07
42	325,000	327,786	50	1248	59	2.75	2.04	164	944	3	16	2.59	59	0.06	0.39
43	325,000	323,992	15	1792	19	7.15	0.96	57	362	4	10	0.37	74	0.00	0.11
44	365,000	286,155	9	273	28	4.92	2.72	131	652	4	9	0.56	25	0.02	0.24
av	*330,000*	*320,350*	*77*	*1568*	*25*	*10.29*	*1.87*	*74*	*746*	*11*	*18*	*0.71*	*53*	*0.02*	*0.39*
σ	*14,393*	*14,474*	*132*	*1694*	*15*	*13.73*	*0.80*	*48*	*625*	*17*	*19*	*0.78*	*35*	*0.02*	*0.53*
m	*325,000*	*323,992*	*20*	*1248*	*21*	*4.92*	*2.04*	*57*	*525*	*4*	*10*	*0.49*	*59*	*0.02*	*0.12*
Alexandrinskoye deposit															
45	325,000	350,470	199	44	15	47.70	4.56	33	440	5	10	0.08	10	0.01	0.00
46	325,000	351,217	101	53	15	89.12	4.63	32	250	17	6	0.19	9	0.01	0.02
47	325,000	348,072	148	52	14	21.07	0.93	32	310	13	7	0.06	13	0.01	0.09

(continued on next page)

Table 5 (*continued*)

	Fe	Cu	Zn	Pb	Sb	Se	Te	As	Mn	Ti	V	Mo	W	U	Tl
av	*325,000*	*349,920*	*149*	*50*	*15*	*68.41*	*3.37*	*32*	*333*	*12*	*8*	*0.11*	*11*	*0.01*	*0.04*
σ	*0*	*1342*	*40*	*4*	*0.47*	*20.71*	*1.73*	*0.47*	*79*	*5*	*2*	*0.06*	*2*	*0.00*	*0.04*
m	*325,000*	*349,919*	*148*	*50*	*15*	*58*	*4.57*	*32*	*310*	*12*	*7*	*0.08*	*10*	*0.01*	*0.02*
av	**328,500**	**329,221**	**99**	**1113**	**22**	**23.21**	**2.32**	**62**	**622**	**11**	**15**	**0.53**	**40**	**0.02**	**0,28**
Pyrite of tube fossils in sulfide ores (n 16)															
Sibai deposit (framboidal pyrite)															
48	460,000	352	110	810	265	0.54	0.10	2172	986	5	9	93	1.12	0.03	44
49	459,000	640	140	1262	399	3.04	0.13	910	1450	5	9	94	1.80	0.03	66
50	459,000	623	136	1125	335	2.16	0.29	1010	1541	5	11	125	1.69	0.02	46
51	457,000	388	271	965	239	0.77	0.49	2054	2912	6	4	47	16.42	0.42	46
52	456,000	748	354	1453	451	1.10	0.00	1965	2577	5	10	285	13.63	0.20	41
53	456,000	729	501	1665	487	3.72	1.03	2353	2410	10	11	146	6.17	0.17	47
54	454,000	942	373	2260	631	1.38	0.00	3104	2124	5	8	261	9.66	0.76	44
55	456,000	1016	481	2152	613	5.32	0.46	1635	1379	5	7	74	28.08	0.05	130
av	*457,125*	*670*	*296*	*1462*	*427*	*2.25*	*0.17*	*1900*	*1922*	*6*	*9*	*141*	*9.82*	*0.21*	*58*
σ	*1900*	*220*	*146*	*497*	*137*	*1.56*	*0.17*	*671*	*635*	*2*	*2*	*82*	*8.74*	*0.24*	*28*
m	*456,500*	*684*	*312*	*1357*	*425*	*1.77*	*0.12*	*2009*	*1832*	*5*	*9*	*110*	*7.91*	*0.11*	*46*
Crystalline pyrite of tube fossils in sulfide ores															
Sibai deposit (crystalline pyrite)															
56	454,000	1543	380	3526	922	3.31	0.08	2086	1478	5	7	32	3.08	0.02	166
57	452,000	1785	413	5014	1161	2.80	0.17	2228	983	6	6	26	1.36	0.02	115
58	456,000	2559	291	5294	1728	2.83	0.11	2357	1101	5	6	104	2.54	0.10	48
59	454,000	1602	461	3996	926	2.64	0.35	1939	928	8	8	28	1.58	0.07	133
60	454,000	1599	467	4056	907	2.44	0.06	1940	830	4	8	30	1.44	0.04	118
61	452,000	1828	430	4492	1444	4.72	0.23	2251	836	5	6	24	1.15	0.03	115
62	454,000	1497	361	3873	960	3.66	0.04	2061	1198	5	7	33	1.93	0.02	149
63	454,000	1438	364	2380	852	5.45	0.18	2829	1626	7	5	188	5.33	0.89	36
av	*453,750*	*1731*	*396*	*4079*	*1112*	*3.48*	*0.12*	*2211*	*1122*	*5*	*7*	*58*	*2.30*	*0.15*	*109*
σ	*1199*	*337*	*55*	*849*	*295*	*1.01*	*0.07*	*272*	*276*	*1*	*1*	*55*	*1.29*	*0.28*	*43*
m	*454,000*	*1601*	*388*	*4026*	*943*	*3.07*	*0.11*	*2149*	*1042*	*5*	*7*	*33*	*1.93*	*0.05*	*115*
av	**455,438**	**1206**	**346**	**2770**	**770**	**2.87**	**0.14**	**2056**	**1522**	**5**	**8**	**99**	**6.06**	**0.18**	**84**
Chlorite of hyaloclasts															
Molodezhnoye deposit															
64	276,000	79	3161	113	40	3.57	4.49	142	16,417	451	3019	0.72	5.29	51	0.07
65	305,000	27	3269	67	39	1.94	0.86	127	8573	433	2128	0.08	4.46	50	0.11
av	*290,500*	*53*	*3215*	*90*	*40*	*2.8*	*2.7*	*135*	*12,495*	*442*	*2573*	*0.40*	*4.8*	*50*	*0.09*

Notes. Av – average value; σ – standard deviation; m – median value.

the high Si cation values (5.00–5.39) and high Fe/(Fe + Mg) (0.799–1.000) and Al^{IV}/Al^{IV} (0.819–0.931) ratios, is associated with quartz, muscovite, chlorite and tourmaline and was formed by hydrothermal replacement of pre-existing muscovite or chlorite. In contrast, our Fe-rich chlorite (chamozite) of tube microfossils and hyaloclasts from gossanites is not associated with hydrothermal or metamorphic silicates and is distinct in specific chemical composition (Table 2). It was previously found that XRD patterns of some chlorites from gossanites show small wide 14-Å peak typical for the presence of smectite layers in chlorites (Ayupova and Maslennikov, 2013). The presence of smectite component is probably responsible for erroneous (overestimated) calculated temperatures of chlorite formation in gossanites.

5.2.3. Illite

The higher K_2O contents in gossanites (0.25–0.83 wt.%, Maslennikov et al., 2012) are related to the presence of illite. Previously, illite was found in association with leucoxene in the silica–hematite matrix of gossanites of the Molodezhnoye deposit (Ayupova and Maslennikov, 2013) and the cement of sulfide sandstones of the Alexandrinskoye deposit. The accumulation of potassium, and formation of illite in the cavities of hematite–chlorite tube microfossils, most likely occurred in the presence of organic matter, which maintains an active energy metabolism (Harder and Dijkhuisen, 1983). This is also confirmed by low $\delta^{34}S$ values of sulfide sandstones from the top of some Uralian VHMS deposits. The formation of clay minerals mediated by microbes follows a complex path involving mixtures of multiple authigenic mineral phases and altered amorphous glass (Alt and Mata, 2000). The smectite-to-illite reaction is closely related to microbial dissolution of smectite through reduction of Fe(III) in the smectite structure (Kim et al., 2004). More likely, the dissolution of multiple units of nontronite precipitates one unit of illite, with excess Si and Fe precipitated as silica and siderite or vivianite, depending on the chemistry of the solution (Kim et al., 2004). The mineral assemblage of chlorite, illite, and Fe oxides, with few carbonates in the cavities of the chlorite–hematite tube microfossils, confirm bacterial activity during formation of illite. Coleman (1985) proposed that calcite will be dissolved to maintain pH; however, where little or no calcite is present H^+ may instead strip micas of their interlayer K ions.

5.2.4. Apatite

The fine clastic hematite–quartz matrix of gossanites hosts rare lithogenic apatite (Ayupova et al., 2011), or bacterial structures replaced by apatite (Maslennikov et al., 2012; Ayupova et al., 2016). The elevated concentrations of phosphorous in these microbial structures are due to its incorporation within the cells. The possibility of phosphorous accumulation in the hematite of tube microfossils (P_2O_5 0.35–0.56 wt.%) is supported by finding of authigenic apatite within the tubes in assemblage with chamosite and illite.

Sedimentary phosphates are usually considered to have formed by microbial activity liberating phosphate during the decomposition of organic compounds (Krajewski et al., 1994). Specifically, microbial redox processes are thought to favor the precipitation of apatite by enhancing chemical gradients and creating pH shifts. Calcium hydroxyapatite is also known to precipitate directly around bacteria (Schmittner and Giresse, 1999) and the tube walls of modern vestimentiferans and alvinellid polychaetes are heavily colonized by bacteria (Shillito et al., 1995). Siliceous–ferruginous sediments from East Blanco Depression

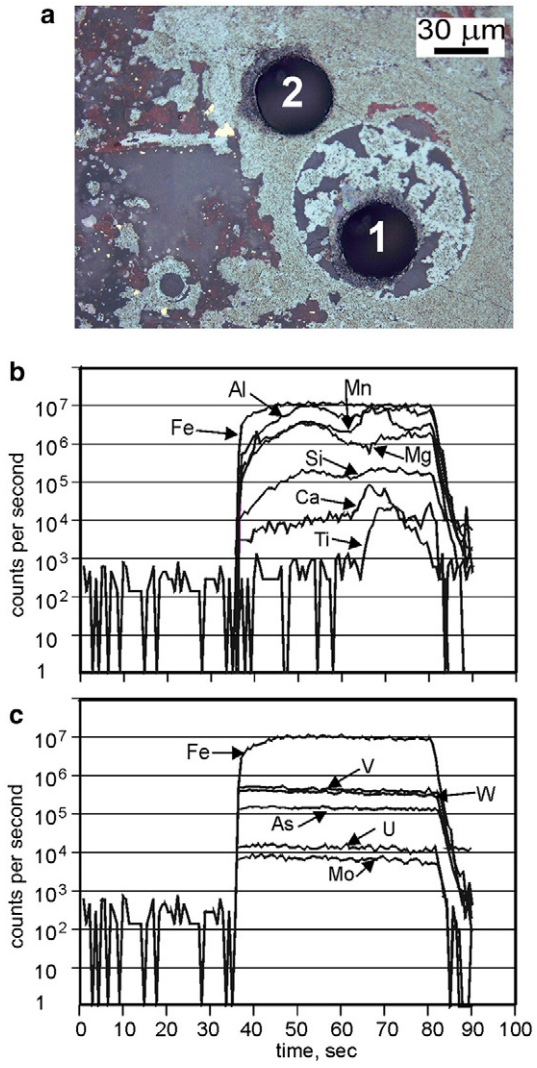

Fig. 10. (a) Points (1 and 2) of LA–ICP–MS analyses in hematite of the tube microfossils and (b, c) representative single-spot LA–ISP–MS spectra of selected elements in this hematite (point 1).

(Northeast Pacific) were formed in excess of the bacterial mat inheriting enrichments in phosphorous (to 2.80 wt.% P_2O_5; Hein et al., 2008).

5.2.5. Titanium-bearing minerals

Under oxidizing conditions, the transformation of hyaloclasts into Si–Fe aggregates is accompanied by the formation of bluish-white aggregates (in dark-field light) enriched in Ti, which are further transformed into anatase (Maslennikov et al., 2012). The quartz matrix locally contains inclusions of the rutile or titanomagnetite aciculae as products of relict hyaloclasts (Ayupova et al., 2011). The processes of complete transformation of hyaloclasts into hematite–quartz aggregates, however, lead to destruction of newly formed Ti minerals (Maslennikov et al., 2012). The Ti^{4+} ions may be mobilized only for short distances beyond the domains of the detrital Ti-bearing minerals because of the low solubility of Ti^{4+} ions in aqueous solutions, so that dissolution and precipitation take place on a scale of centimetres rather than meters (Morad, 1988). The formation of authigenic anatase as a result of post-depositional migration of titanium is known from deep-sea sediment and interstitial water (Correns, 1954).

However, the studied gossanites contain atypical leucoxene aggregates in both the tube cavities and around tube microfossils (Fig. 5d, f), as well as unique microstromatolitic leucoxene aggregates (Fig. 6d). Thus, titaniumin gossanites may be of both lithogenic and biogenic origin similarly to marine sediments (Correns, 1954; Orians et al., 1990). Titanium can be derived from the alteration of hyaloclasts during the early stages of diagenesis and is related to the decomposition of organic material (Grey and Reid, 1975). Probably, biogenic titanium is scavenged by colloidal iron that is taken up by the tube organisms during formation of the gossanites. During successive diagenetic alteration, the "amorphous" phases of stromatolites recrystallize into minerals with a crystalline structure often acting as cement. An assemblage of leucoxene and chlorite (chamosite) indicates the relatively low-temperature diagenetic conditions during their formation. The association of leucoxene with tube microfossils are highly important, since little is known on the biophile properties of titanium. Some organisms can consume soluble forms of titanium (Konhauser, 2006), and it can be passively accumulated during the etching of oceanic basaltic glass by microbes (Banerjee et al., 2006, 2010). Furthermore, the presence of rutile crystals inside foraminiferal species *Bathysipphon argenteus* indicates the possibility of Ti concentration in biogenic textures (Dick, 1928).

5.2.6. Carbonates

Carbonates in gossanites occur as cements, clasts or microfossils. It is suggested that in the tube worms, carbonates replace stabilizing easily decomposed chitin microfibrils (Lowenstam and Weiner, 1989; Reitner, 1993). Moreover, acidic glycoproteins liberated during degradation might have acted as a matrix for initial carbonate mineralization (Lowenstam and Weiner, 1989). Zonation of carbonates inside the tubes most likely reflects their primary bio-mineralogical pattern - probably, alternation of calcite and aragonite layers.

Incorporation of Mg, Mn, andFe in the composition of ankerite suggests a process of microbial Fe(III) oxidation (Sposito, 1984). With an increased burial temperature, organic matter begins to be decomposed by chemical rather than biological processes. Under anoxic conditions and low sulfate concentrations, the formation of dolomite/ankerite and siderite is expected (Gautier and Claypool, 1984). The siderite would have been formed by an increase in the P_{CO2} during biological sulfate reduction, and the finely laminated textures likely represent replaced biogenic mats (Tornos et al., 2008).

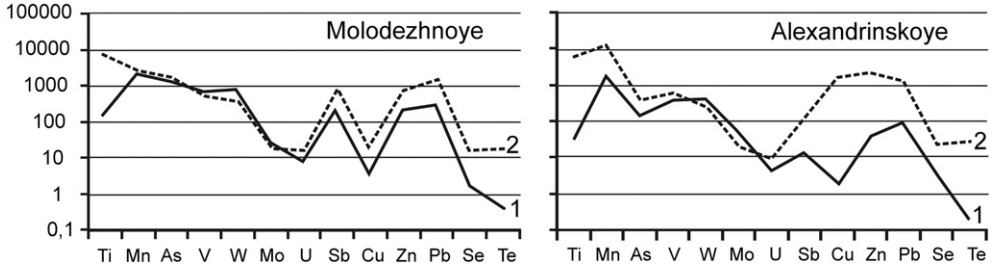

Fig. 11. Trace element patterns (average, ppm) in hematite of the tube microfossils (1) and pseudomorphic hematite (2) from Molodezhnoye and Alexandrinskoye deposits.

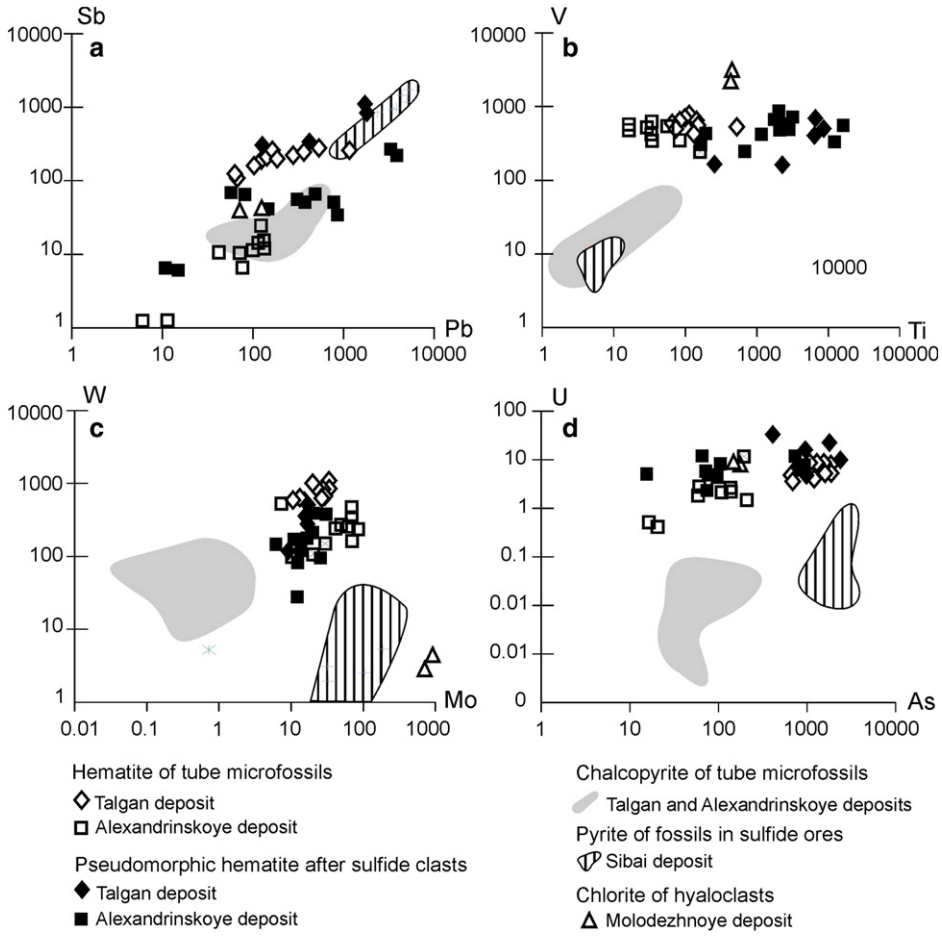

Fig. 12. Trace elements distribution in hematite and chalcopyrite of the tube microfossils, pseudomorphic hematite after sulfides, and chlorite of hyaloclasts from gossanites and pyrite of tube fossils from sulfide ores. Talgan, Alexandrinskoye, Sibai and Molodezhnoye deposits.

Monheimite with 23 wt.% FeO was formed from carbon dioxide fluids during submarine weathering of sulfide ores with Fe-bearing sphalerite; it often replaced earlier carbonates at pH of >7 (Ayupova et al., 2011).

The precipitation of dolomite in the presence of bacteria (Vasconcelos et al., 1995) also suggests diagenetic environments owing to an effective migration and mixing of pore water due to the compaction of sediments. Direct precipitation of dolomite is also known to take place when supersaturation overcomes low-temperature kinetic barriers (e.g., Aloisi et al., 2000). Dolomite precipitation is favored when sulfate is removed from the pore water by intense sulfate reducing microbial activity (Kelts and McKenzie, 1982).

Siderite is likely to be a product of organic matter oxidation coupled with the reduction of Fe(III) biominerals through either microbial or abiotic thermal processes. The spherical forms associated with oxidized pyrite framboids are interpreted to be the result of sulfur-oxidizing bacteria. At temperatures of 60–120 °C, numerical estimations show that if the ΣH_2S content is relatively low and the pH is mildly acidic (≈4.5–5.5), then siderite is stable together with pyrite (Stetter et al., 1990).

5.3. Stable isotopes as indicator of biological processes

The carbon isotopic composition of carbonates associated with tube microfossils (−4.2 to −26.2‰) are much lower than those for carbonates precipitated from seawater (e.g. crinoid-bearing carbonate clasts), and are indicative of biological activity. Similar negative $\delta^{13}C$ values have been determined for calcite from the axial part of the vestimentiferan tubes of the Sibai deposit (Table 4) (Maslennikov, 1999). These values span a range of the $\delta^{13}C$ values of the hydrothermal vent tube worms from the rift zones of the Pacific Ocean (−11 to −14‰), whose trophosome tissue contains several enzymes associated with a chemoautotrophic existence (Felbeck, 1981; Gal'chenko et al., 1988).

The fractionation of carbon isotopes during the oxidation of dissolved organic matter by bacteria has previously been used to explain the depleted $\delta^{13}C$ ratios in glass suspected to have been biogenically altered (Furnes et al., 2001). The $\delta^{13}C$ values of calcites (−19.7 to −10.8‰) and rhodochrosite (−28.1 to −12.8‰) are typical of authigenic carbonates from Paleozoic manganese deposits of the Urals (Brusnitsyn and Zhukov, 2012).

In our case, the carbon isotopic composition may be caused by the intensity of the diagenetic process and the amount of sedimentary carbonate in the oxide–ferruginous sediments. However, in some cases, extremely light values (up to −26.2‰) exceed those established for biogenic facies of modern hydrothermal systems. It is known that the metabolic activity of iron oxidizing bacteria produces organic matter with $\delta^{13}C$ of −26.8‰ (e.g., Holm, 1988). Similarly, light $\delta^{13}C$ values ranging from −27.2 to −8.1‰ were reported for goethite, which may indicate that carbon isotopic values are able to withstand iron oxide phase transitions (Yapp and Poths, 1986).The light $\delta^{13}C$ values, however, could also reflect primary conditions.

The authigenic carbonates and carbonate clasts in gossanites show the high $\delta^{18}O$ values (+8 to +16.68‰) in contrast to that of the Devonian seawater (0 ± 1‰ VSMOW) (Muehlenbachs et al., 2003). Large variations in $\delta^{18}O$ data may reflect diagenetic alteration (Jaffrés et al., 2007).

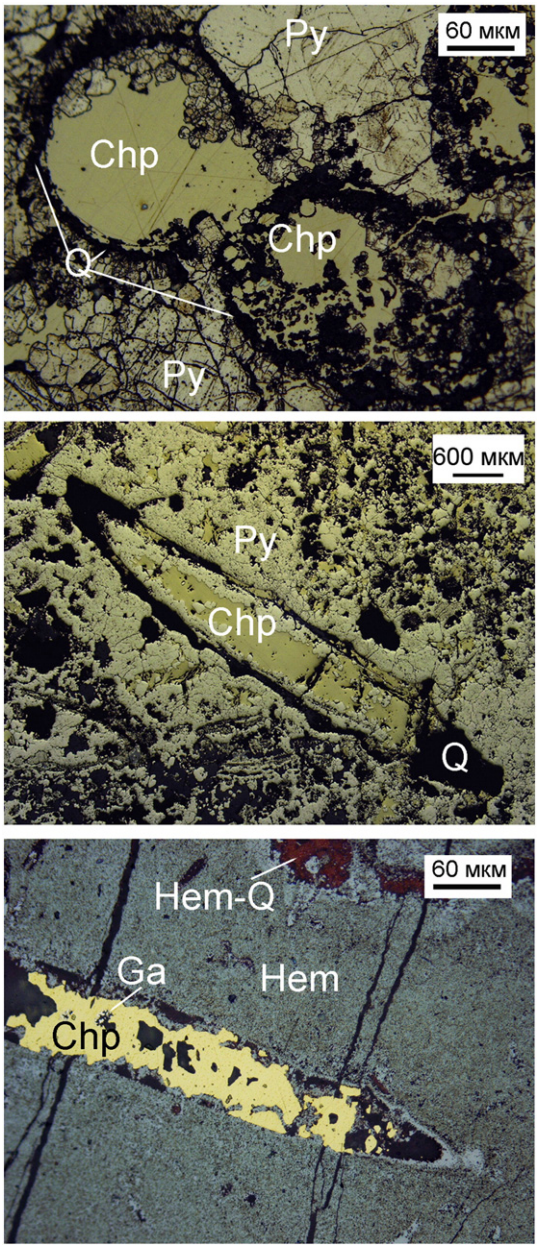

Fig. 13. Transverse (a) and oblique (b, c) sections of sulfidized tube microfossils in clastic sulfide ores of the Novo-Shemur (a) and Priorskoye (b) deposits and gossanites of the Talgan (c) deposit: a, b – tube microfossil with outer quartz wall, inner wall incrusted by crystalline pyrite, and chalcopyrite filling; c – tube microfossil with outer and inner hematite walls with quartz layer and chalcopyrite filling. Wavy surface may indicate segmentation of the body of the tube microfossils. Chp – chalcopyrite, Py – pyrite, Q – quartz, Hem – hematite, Hem + Q –hematite–quartz aggregates. Reflected light images.

The temperature of formation of these carbonates can be estimated knowing the isotopic composition of the fluid. The estimated formation temperatures of our carbonates varied from ~70 to 166 °C (Fig. 9) correspond to a temperature range of activity of mesophilic and thermophilic microorganisms (20–150 °C) (Stetter et al., 1990). The temperature calculation can be applied to natural biogenic carbonate systems, however, this application is questionable. According to Kim and O'Neil (1997), "all else being equal, a change of 1 per mil in $\delta^{18}O$ of nonequilibrium carbonate would correspond to a change of about 3 °C, whereas the same change in $\delta^{18}O$ for an equilibrium carbonate would correspond to a change of about 4 °C". Assuming these data, we can suggest that the temperature of formation of our carbonates vary from ~5 to 130 °C. Several samples with higher temperatures (up to 166 °C) do not

Table 6
Mineral succession for precursor and authigenic minerals and pH parameters of formation conditions of mineral assemblages.

Process	Mineral succession	pH
Sulfide oxidation	Sulfide clasts → amorphous iron oxi-hydroxides ($\pm$*Cu,Pb,Zn,As,Sb; +Mn,V,W,Mo,U*) → hematite ($\pm$*Cu,Pb,Zn,Sb + As,Mn,V,W,Mo,U*)	> ~ 4
Hyaloclast destruction	Hyaloclasts → nontronite?(+*Ti,V,Mn*) → $mFe_2O_3 \cdot nSiO_2 \cdot pH_2O$ (hisingerite?) (+*Ti,V,Mn*) → hematite (+*V,Mn*) + quartz + anatase	> ~ 4
Formation of hematite tube microfossils	Amorphous iron oxi-hydroxides ($\pm$*Pb,Sb,As,V,W,Mo,U*) ± SiO_2 nH_2O ± $TiO_2 \cdot nH_2O$ ± amorphous calcium phosphate → hematite (+*As,Pb,Sb,V,W,Mo,U*) ± apatite ± leucoxene ± quartz	≥6
Formation of hematite–chlorite tube microfossils	*nontronite ($\pm$ *K*) + **amorphous oxi-hydroxides (+*As,Pb,Sb,V,W,Mo,U*) ± SiO_2 nH_2O ± **$TiO_2 \cdot nH_2O$ ± **amorphous calcium phosphate → chamozite ± illite + apatite + hematite (+*As,Pb,Sb,V,W,Mo,U*) + quartz + leucoxene	* ≤ 6 ** ≥ 6
Formation of carbonate–hematite tube microfossils	(Mn,Fe/Mg/Zn)-rich aragonite? ± amorphous oxi-hydroxides (+*V*) ± SiO_2 nH_2O + amorphous calcium phosphate + $TiO_2 \cdot nH_2O$ → Mn-bearing calcite, ankerite, siderite, dolomite, monheimite ± hematite + quartz + leucoxene	≥7

Note. Table is compiled on the basis of data from (Drennan, 1964; Maynard, 1983; Morad, 1988; Stetter et al., 1990; Needham et al., 2004; Banerjee et al., 2006, 2010; Alt and Mata, 2000; Himmler et al., 2011; Maslennikov et al., 2012).
* – pH ≤ 6, ** – pH ≥ 6.

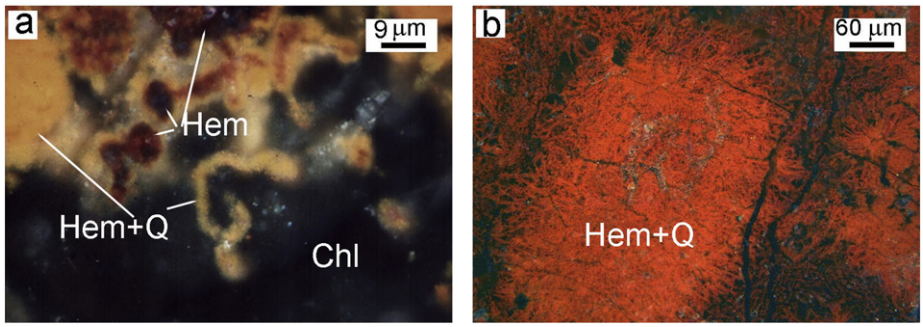

Fig. 14. Hematitized filaments surround partially (a) and completely (b) oxidized hyaloclasts in gossanites. Molodezhnoye (a) and Talgan (b) deposit. Hem – hematite, Chl – chlorite, Hem–Q – hematite + quartz aggregates.

correspond to this range and could probably be explained by isotopic exchange and further increase in formation temperature of carbonates when seawater is modified by chemical exchange with volcanic glass (Torsvik et al., 1998).

5.4. Trace elements in hematite

The elevated metal contents in hematite of tube microfossils are also typical of modern tube worms (Lein et al., 1989; Juniper et al., 1992; Demina et al., 2007), as well as of sulfidized polychaetes from the Uralian VHMS deposits (Table 5). The fossilization and preservation of microbial mats within iron–silica deposits also occurs at modern hydrothermal fields. Most Fe-Si oxyhydroxide deposits are derived from the leaching of basaltic rocks, with sediments being the main source of some trace elements (e.g., U, As, Mo). For example, siliceous–ferruginous sediments from East Blanco Depression (Northeast Pacific) were formed in excess of the bacterial mat inheriting enrichments in Mn (to 2.23 wt.%), As (to 194 ppm), V (to 292 ppm), Mo (to 109 ppm), and U (to 51 ppm) (Hein et al., 2008). The enrichment in biophile elements such as P, Fe, Mn, As, Cu, Mg, and Zn is a characteristic of bacterial activity associated with the formation of black shale-hosted Mn carbonate deposits (Polgári et al., 2012). Sediments in anoxic environments are generally enriched in V, Mo, W, Cu, Zn, and Pb over those deposited under oxic conditions. The latter are also enriched in Mn (Calvert and Pederson, 1993).

As the trace element composition of pseudomorphic hematite and hematite of tube microfossils is similar, it is impossible to conclude whether the biogenic or mechanical sorption of metals and metalloids was responsible. The accumulation of these elements in hematite may be related to the ability of fine particles of precursor iron hydroxides to incorporate the metals and metalloids in their structure (Watson, 1996). It is known, however, that organo-mineral complexes of iron hydroxides are better sorbents relative to ferrihydrite, and the higher the content of organic carbon the better the sorption (Zhu et al., 2011).

It was previously established that Cu, Pb, Zn, As, Se, and Te were removed from sulfide clasts during seafloor oxidation and redeposited in pseudomorphic hematite after sulfide clasts that locally led to the formation of rare authigenic mineral assemblages (Ayupova et al., 2015). The enrichment of pseudomorphic hematite in these elements depends on the composition of the sulfide ores, which can change due to submarine alteration processes. As an example, the gossanites from the Alexandrinskoye deposit contain several pseudomorphs after sphalerite clasts, which was causing high Zn contents in pseudomorphic hematite. The extremely low contents of chalcophile elements in biomorphic hematite are best explained by their sorption by iron oxyhydroxides from the fluids (except for As). Below, we discuss in detail the trace elements displaying high contents in biomorphic hematite (As, Mn, W, V, Mo, U).

Arsenic. Hematite of tube microfossils and pseudomorphic hematite after sulfide clasts are enriched in As that is explained by strong affinity of arsenate As(V) and arsenite As(III) to iron oxides. The As(V) ions are stable under reducing conditions and form robust bidentant complexes with intraspherical fixation on the particles of iron hydroxides (Pactung et al., 2003). An increase in pH (from 3 to 10) leads to a decrease in the amount of absorbed arsenate on iron hydroxides, whereas the amount of absorbed arsenite increases to a maximum at a pH of 9 (Jain and Loeppert, 2004). In neutral conditions, As(III) is more steadily fixed on the surface of iron hydroxide relative to As(V) (Manning and Goldberg, 1996). Active microbial metabolism results in the formation of biogenic iron hydroxides, which incorporate toxic As(III) into its structure or absorb it on to the surface (Morin et al., 2003). Some microbes exposed to arsenic employ mobile genetic structures (plasmids) to manufacture proteins that (although counterintuitive) reducing the less toxic As(V) to more toxic As(3) and secrete it from their cells (Rahman and Hassler, 2014). Other oxyanions (PO_4^{3-}, SO_4^{2-}, MoO_4^{2-}) prevent the robust fixation of arsenic (Manning and Goldberg, 1996).

Arsenic, along with phosphorous, is concentrated in biomorphic hematite filling the tube microfossils and is probably an important component of the biomineralization process. It was found that arsenic is a chemical analogue of phosphorous and can substitute for phosphorous under its deficit during intracellular biochemical reactions (Wolfe-Simon et al., 2010). Various organisms have developed methods, through which they may volatilize and mineralize toxic compounds in their aquatic environment (Pracejus and Halbach, 1996). This reduces the activity/concentration of the respective toxic compound in the environment, even if the individual organism eventually dies. The colloform aggregates and filamentous orpiment (typical features of fungal organisms) were found in sulfide–sulfate samples from seafloor hydrothermal fields (Dekov et al., 2013). Because of its high toxicity, the habitat polluted by arsenic is characterized by low species diversity that was probably reflected on the absence of other species with As-bearing tube microfossils in gossanites from the studied VHMS deposits.

Manganese is a typical isomorphic element of iron oxyhydroxides. The high Mn contents in hematite of the tube microfossils correlate with high Ca contents, as this hematite contains microinclusions of Mn-bearing carbonates. The high Mn contents are also characteristic of pyritized polychaetes from the sulfide ores that is related to Mn oxides within tubes (Maslennikov, 1999). Late Mn-rich chalcopyrite of tubes inherits Mn from the cavities of the tubes. Chlorite from hyaloclasts also contains high Mn contents (Table 5). Manganese promotes the degradation of a wide array of complex organics via multiple chemical mechanisms (Ulrich and Stone, 1989).

Oxidation of sulfides is accompanied by an enrichment in Mn and, locally, its contents in pseudomorphic hematite exceed those in hematite of tube microfossils by one order of magnitude (Table 5). In sulfide ores, Mn is typically concentrated in hydrothermal sedimentary colloform pyrite (av. 500–700 ppm Mn) (Maslennikova and Maslennikov, 2007). Thus, sulfide ores are one of the sources of Mn for gossanites. The Mn oxide deposits occur along the margins of black shale-hosted Mn carbonate deposits formed by bacterially mediated diagenetic processes (Polgári et al., 2012).

Tungsten, vanadium, and molybdenum. The high W, V, and Mo contents in biomorphic hematite are of special interest. In spite of extremely low W and V contents in sulfides from VHMS deposits (0–30 ppm,

Maslennikov et al., 2014), hematite of tube microfossils and pseudomorphic hematite after sulfide clasts contain high amounts of these elements (Table 5). Chlorite of hyaloclasts is a source of V for iron oxyhydroxides because of the high contents of this element. However, despite the high Mo contents in sulfides from smoker chimneys (e.g., up to 149 ppm Mo in chalcopyrite of the Alexandrinskoye deposit, Maslennikov et al., 2014), its contents in pseudomorphic hematite after sulfide clasts are lower relative to hematite of tube microfossils (Table 5).

Experimentally supported intraspherical and surface sorption of WO_4^{2-} and MoO_4^{2-}, respectively, by iron oxyhydroxides causes different behavior of these elements on the surface of Fe oxyhydroxides (Kashiwabara et al., 2013). The W contents, which are higher than Mo contents by one order of magnitude, are probably explained by the intraspherically-absorbed WO_4^{2-} ions which are much more steadily fixed in iron oxyhydroxides than MoO_4^{2-} ions, which are fixed by ionic exchange. It has been suggested that W may be associated with Mn in form of $MnWO_4$ (Kashiwabara et al., 2013). Organic matter is a suitable substrate for Mo scavenging (Lyonsa et al., 2003).

W and Mo are redox-sensitive trace metals with many stable isotopes, which lead to their variable chemistry and isotopic ratios in geochemical and biological systems (e.g., Kletzin and Adams, 1996). Tungsten and vanadium in carbon-bearing sediments are considered the physiological relics of the Early Archean biosphere involved, along with Fe, in biological circulation (Kletzin and Adams, 1996). The bioorganic ellipsoids and associated minerals of Mo from ore samples of early Cambrian black shales (South China) present evidence for biotic involvement during mineralization processes (Shi et al., 2014). It is considered that molybdenum was inaccessible in the oxygen-free biosphere of the early Earth and its functions were performed by other metals (e.g., W, V or even Fe) (Kletzin and Adams, 1996). This suggestion is supported by distribution of bacteria with corresponding ferments along the geochemical gradients around the modern hydrothermal vents: the hydrothermal fauna inhabited by hyperthermophiles is rich in W and is depleted in Mo, which precipitates as sulfide (Gallant and von Damm, 2001). It is believed that, toward from H_2S-saturated hydrotherms, Mo becomes soluble in the presence of oxygen, whereas W becomes inaccessible for metabolic processes and, correspondingly, the composition of microbial communities varies, where Mo substitutes W in exchange processes (Adams et al., 1998). This is also typical of the Devonian hydrothermal–biogenic ecosystems of the Urals massive sulfide deposits (Maslennikov, 2006). Vanadium trapped by organic matter may precipitate along with it and may be partially absorbed by $Fe(OH)_3$ or $SiO_2 \times nH_2O$ gels (Emel'yanov et al., 1979).

Uranium. Surprisingly, the high U contents in the studied samples are typical of pseudomorphic hematite after sulfide clasts (up to 22.59 ppm) and authigenic chlorite (up to 51 ppm) formed during the transformation of hyaloclasts (cf., Maslennikov et al., 2012) rather than of hematite of tube microfossils. In modern environments, high U contents were detected in metalliferous sediments from the Juan de Fuca Ridge (up to 30 ppm) (Hrischeva and Scott, 2007) and the TAG field of the Mid-Atlantic Ridge (up to 20 ppm) (Mills et al., 1994). Iron sulfides from the Semenov-1 hydrothermal field (Mid-Atlantic Ridge) contains up to 11 ppm U (Melekestseva et al., 2014). These occurrences have been attributed to fixation of seawater-derived U during the oxidation of iron sulfide, possibly through microbially mediated reactions (Mills et al., 1994; Hrischeva and Scott, 2007). However, the high U contents (up to 50 ppm) in hyaloclasts (Table 5) suggest that hyaloclastites are the additional U sources for our hematite. Microbes immobilize U by intra- and extracellular precipitation of secondary minerals (Jeong et al., 1997).

6. Conclusions

1) Tube microfossils from hematite (hematite–quartz), hematite–chlorite and carbonate–gossanites of the Uralian VHMS deposits studied are distinct in occurrence, morphology, internal structure, and mineralization. They may be ascribed to siboglinids, polychaetes, and calcerous serpulids, respectively. Their mineralization reflects the primary mineral composition of sulfide–hyaloclast–carbonate substrate responsible for the formation of gossanites. The Fe-oxides, Fe-aluminosilicates and Fe-carbonates are dominant minerals responsible for replicating delicate tissues during diagenesis. The well-preserved microfossils indicate diagenetic transformation of primary sediments.
2) The morphological and structural features of the tube microfossils, filaments, thin films and spherical bodies are strong evidence for their organic origin rather than the products of inorganic precipitation during the formation of the gossanites. Each type of tube microfossil is characterized by specific bacterial assemblages. Preservation of bacteria is related to the rapid fossilization of the tube structures, which occurred prior to the beginning of degradation of the bacterial bodies. Bacterial decomposition of organic matter plays an important role in fossil diagenesis, controlling pH, Eh, and form of mineral assemblages during fossilization.
   The major authigenic minerals of the tube microfossils (hematite, quartz, chlorite, illite, carbonates, apatite, and leucoxene) are responsible for the fossilization of chitin and soft tissue of the tube worms in gossanites. The type of minerals mainly depends on the composition of the sediments (sulfides, hyaloclasts, carbonates) and the ambient conditions created by their decay. There is evidence for both abiotic mineral precipitation and biologically induced mineral precipitation processes within this system.
4) The carbon isotopic composition of carbonates associated with tube microfossils is indicative of biological activity and is caused by the intensity of diagenetic process and the amount of sedimentary carbonate in oxide–ferruginous sediments. The extremely light values ($\delta^{13}C$ up to −26.2‰) could reflect primary sedimentation conditions. The oxygen isotopic composition of carbonates associated with tube microfossils is similar in all three types of rocks due to active sulfate reduction during diagenesis (and anadiagenesis) of sediments. The formation temperatures of studied carbonates vary from 70 to 166 °C and the elevated temperatures could be explained by isotopic exchange and further increase in formation temperature of carbonates when seawater is modified by chemical exchange with volcanic glass.
6) The trace element composition of hematite of tube microfossils and pseudomorphic hematite after sulfides is similar and may be related to the ability of fine particles of precursor iron hydroxides to incorporate the released metals in structure during the oxidation of iron sulfides and decomposition of hyaloclasts, possibly, through microbially-mediated reactions. The extremely low contents of chalcophile elements in biomorphic hematite are explained by their sorption to iron oxyhydroxides from the fluids, except for As. Arsenic, along with phosphorous, is concentrated in biomorphic hematite, which fills the tube microfossils, and is probably an important component of the biomineralization process.
7) The discovery of tube microfossils in gossanites is important indicator of ancient habitats in iron–silica-rich rocks associated with VHMS deposits. This detailed study of their mineral and chemical composition may influence the interpretation of genetic features of these rocks associated with VHMS deposits worldwide.

Supplementary data to this article can be found online at http://dx.doi.org/10.1016/j.oregeorev.2016.08.003.

Acknowledgments

The authors thank Irina Melekestseva for help in preparation of the manuscprit. The mineralogical and isotopic studies were supported by the State Contract of the Institute of Mineralogy UB RAS № AAAA-

A16-116021010244-0 and Presidium UB RAS (program no. 15-11-5-23). The geochemical studies were supported by the Russian Science Foundation (project no. 14-17-00691). SPH is currently supported by the Irish Centre for Research in Applied Geosciences (iCRAG). iCRAG is funded under the Science Foundation Ireland Research Centres Programme and is co-funded under the European Regional Development Fund. We are grateful to Dr. Márta Polgári, one anonymous reviewer and managing guest editor of Ore Geology Reviews O.Yu. Plotinskaya for their detailed and constructive reviews, which helped us greatly to improve this paper.

References

Adachi, M., Yamamoto, K., Sugisaki, R., 1986. Hydrothermal cherts and associated siliceous rocks from the northern Pacific: Their geological significance as indication of ocean ridge activity. Sediment. Geol. 47, 125–148.

Adams, M.W.W., Wiegel, J., Adams, M.W.W., 1998. The evolutionary significance of the metabolism of tungsten by microorganisms growing at 100 °C. Thermophiles: the key to molecular evolution and the origin of life. Taylor and Francis, London (346 pp.).

Allison, P.A., 1988. The role of anoxia in the decay and mineralization of proteinaceous macrofossils. Paleobiology 14, 139–154.

Aloisi, G., Pierre, C., Rouchy, J.M., Foucher, J.P., Woodside, J., Party, M.S., 2000. Methane related authigenic carbonates of eastern Mediterranean Sea mud volcanoes and their possible relation to gas hydrate destabilisation. Earth Planet. Sci. Lett. 184, 321–338.

Alt, J.C., 1988. Hydrothermal oxide and nontronite deposits on seamounts in the Eastern Pacific. Mar. Geol. 81, 227–239.

Alt, J.C., Mata, P., 2000. On the role of microbes in the alteration of submarine basaltic glass: A TEM study. Earth Planet. Sci. Lett. 181, 301–313.

Ayupova, N.R., Maslennikov, V.V., 2012. Biomineralization in ferruginous–siliceous sediments of massive sulfide deposits of the Urals. Dokl. Earth Sci. 442 (2), 193–195.

Ayupova, N.R., Maslennikov, V.V., 2013. Biomorphic textures in the ferruginous–siliceous rocks of massive sulfide bearing paleohydrothermal fields in the Urals. Lithol. Miner. Resour. 48, 438–455.

Ayupova, N.R., Novoselov, K.A., Belogub, E.V., 2011. Ferruginous-siliceous sediments are the indicators of massive-sulfide deposits (on exsample of Babaryk ore field, Southern Urals). Lithosphere 3, 117–134 in Russian with English abstract.

Ayupova, N.R., Maslennikov, V.V., Maslennikova, S.P., Blinov, I.A., Danyushevsky, L.V., Large, R.R., 2015. Rare Mineral and Trace Element Assemblages in Submarine Supergene Zone at the Devonian Molodezhnoye VMS Deposit, the Urals, Russia. Proceedings of the 13 SGA Biennial Meeting.Mineral resources in a sustainable world. Université de Lorraine, Nancy, France, pp. 2051–2054.

Ayupova, N.R., Maslennikov, V.V., Sadykov, S.A., Maslennikova, S.P., Danyushevsky, L.V., 2016. Evidence of biogenic activity in quartz-hematite rocks of the Urals VMS deposits. In: Frank-Kamenetskaya, O.V., et al. (Eds.), Biogenic–abiogenic interactions in natural and anthropogenic systems. Springer International Publishing, Switzerland, pp. 109–122.

Banerjee, N.R., Furnes, H., Muehlenbachs, K., Staudigel, H., de Wit, M., 2006. Preservation of 3.4–3.5 Ga microbial biomarkers in pillow lavas and hyaloclastites from the Barberton Greenstone Belt, South Africa.Earth Planet. Sci. Lett. 241, 707–722.

Banerjee, N.R., Izawa, M.R.M., Sapers, H.M., Whitehouse, M.J., 2010. Geochemical biosignatures preserved in microbially altered basaltic glass. Surf. Interface Anal. 43, 452–457.

Berg, I.A., Kockelkorn, D., Ramos-Vera, W.H., Say, R.F., Zarzycki, J., Hügler, M., Alber, B.E., Fuchs, G., 2010. Autotrophic carbon fixation in archaea.Nat. Rev. Microbiol. 8 (6), 447–460.

Bourdelle, F., 2011. Thermobarom'etrie des phylloscilicates dans les s'eries naturelles : conditions de la diag'en'ese et du m'etamorphisme de bas degr'e. Sciences de la TerreUniversit'e Paris Sud - Paris XI, Fran¸cais (https://tel.archives-ouvertes.fr/tel-00616543).

Briggs, D.E.G., Raiswell, R., Bottrell, S.H., Hatfield, D., Bartels, C., 1996. Controls on the pyritization on exceptionally preserved fossils: an analysis of the Lower Devonian Hunsruck Slate of Germany. Am. J. Sci. 296, 633–663.

Brusnitsyn, A.I., Zhukov, I.G., 2012. Manganese deposits of the Devonian Magnitogorsk palaeovolcanic belt (Southern Urals, Russia). Ore Geol. Rev. 47, 42–58.

Calvert, S.E., Pederson, T.F., 1993. Geochemistry of recent oxic and anoxic marine sediments: Implications for the geological record. Mar. Geol. 113, 67–88.

Cathelineau, M., 1988. Cation site occupancy in chlorites and illites as a function of temperature. Clay Miner. 23, 471–485.

Coleman, M.L., 1985. Geochemistry of diagenetic non-silicate minerals: kinetic considerations. Phil. Trans. R. Soc. A 315, 39–55.

Constantinou, G., Govett, G.J.S., 1973. Geology, geochemistry, and genesis of Cyprus sulfide deposits. Econ. Geol. 68, 843–858.

Correns, C.W., 1954. Titan in tiefsee-sedimenten. Deep-Sea Res. 1, 78–85.

Danyushevsky, L., Robinson, P., Gilbert, S., Norman, M., Large, R., McGoldrick, P., Shelley, M., 2011. Routine quantitative multi-element analysis of sulphide minerals by laser ablation ICP–MS: Standard development and consideration of matrix effects. Geochim: Explor. Environ. Anal. 11, 51–60.

Deer, W.A., Howie, R.A., Zussman, J., 1962. Rock-forming minerals.Layered silicates excluding micas and clay minerals.V. 3B. The Geological Society, London 314pp.

Dekov, V.M., Bindi, L., Burgaud, G., Petersen, S., Asael, D., Rédou, V., Fouquet, Y., Pracejus, B., 2013. Inorganic and biogenic As-sulfide precipitation at seafloor hydrothermal fields. Mar. Geol. 342, 28–38.

Demina, L.L., Galkin, S.V., Lein, A.Y., Lisitsyn, A.P., 2007. First data on microelemental composition of benthic organismsfrom the 9°50′ N hydrothermal field, East Pacific Rise. Dokl. Earth Sci. 415 (6), 905–907.

Dick, A.B., 1928. On needles of rutile in the test of Bathysiphon argenteus. Edinburgh Geol. Soc. Trans. 12, 19–21.

Drennan, J.A., 1964. An unusual occurrence of chamosite.Research Department, Coronation Brick & Tile. Clay Min. Bull. 5, 382–391.

Drits, V.A., Ivanovskaya, T.A., Sakharov, B.A., Gor'kova, N.V., Karpova, G.V., Pokrovskaya, E.V., 2001. Pseudomorphous Replacement of Globular Glauconite by Mixed-Layer Chlorite–Berthierine in the Outer Contact of Dike: Evidence from the Lower Riphean Ust'-Il'ya Formation, Anabar Uplift. Lithol. Miner. Resour. 36 (4), 337–352.

Dubinina, G.A., 1978. Mechanism of ferrous iron and manganese oxidation by iron bacteria at neutral acide conditions. Microbiology 47 (4), 591–599.

Duhing, N.C., Stolz, J., Davidson, G.J., Large, R.R., 1992. Cambrian microbial and silica gel textures in silica iron exhalites from the Mount Windsor volcanic belt, Australia: Their petrography, chemistry, and origin. Econ. Geol. 87, 764–784.

Emel'yanov, E.M., Mitropol'skii, A.Y., Shimkus, K.M., Mussa, A.A., 1979. Geochemistry of the Mediterranean Sea. Naukova dumka, Kiev (132 pp. *(in Russian)*.

Emerson, D., Moyer, C.L., 2002. Neutrophilic Fe-oxidizing bacteria are abundant at the Loihi Seamount hydrothermal vents and play a major role in Fe oxide deposition. Appl. Environ. Microbiol. 68, 3085–3093.

Felbeck, H., 1981. Chemoautotrophic potential of the hydrothermal vent tube worm *Riftia pachyptila* Jones (Vestimentifera). Science 213, 336–338.

Ferris, F.G., Beveridge, T.J., Fyfe, W.S., 1986. Iron-silica crystallite nucleation by bacteria in a geothermal sediment. Nature 320, 609–611.

Ferris, F.G., Fyfe, W.S., Beveridge, T.J., 1987. Bacteria as nucleation sites for authigenic minerals in a metal-contaminated lake sediment. Chem. Geol. 63, 225–232.

Frankel, R.B., Papaefthymiou, G.G., Blakemore, R.R., O'Brien, W., 1983. Fe_2O_3 preparition in magnetotactic bacteria. Biochim. Biophys. Acta 763, 147–159.

Furnes, H., Muehlenbachs, K., Torsvik, T., Thorseth, I.H., Tumyr, O., 2001. Microbial fractionation of carbon isotopes in altered basaltic glass from the Atlantic Ocean, Lau Basin and Costa Rica Rift. Chem. Geol. 173, 313–330.

Gal'chenko, V.F., Galkin, S.V., Lein, A.Y., Moskalev, L.I., Ivanov, M.V., 1988. A role of symbiotic bacteria in nutrition of invertebrates from active submarine hydrotherms. Okeanologiya 28 (6), 1020–1031 in Russian.

Gallant, R.M., Von Damm, K.L., 2001. Tungsten and Molybdenum in Seafloor Hydrothermal Systems – as Possible Controls on Biological Communities. American Geophysical Union, Fall Meeting 2001, abstract #OS41A-0442.

Gautier, D.L., Claypool, G.E., 1984. Interpretation of methanic diagenesis in ancient sediments by analogy with processes in modem diagenetic environments. In: McDonald, D.A., Surdam, R.C. (Eds.), Clastic Diagenesis. AAPG Mem. 37, pp. 111–123.

Grenne, T., Slack, J.F., 2003. Bedded jaspers of the Ordovician Lökken ophiolite, Norway: seafloor deposition and diagenetic maturation of hydrothermal plume-derived silica-iron gels. Mineral Deposits 38, 625–639.

Grey, I.F., Reid, A.F., 1975. The structure of pseudorutile and its role in the natural alteration of ilmenite. Am. Minerol. 60, 898–906.

Halbach, M., Halbach, P., Lueders, V., 2002. Sulfide-impregnated and pure silica precipitates of hydrothermal origin from the central Indian Ocean. Chem. Geol. 182, 357–375.

Hannington, M., Jonasson, I., 1992. Fe and Mn oxides at seafloor hydrothermal vents. Catena Suppl. 21, 351–370.

Hannington, M.D., Thompson, G., Rona, P.A., Scott, S.D., 1988. Gold and native copper in supergene sulphides from the Mid-Atlantic Ridge. Nature 333, 64–66.

Harder, W., Dijkhuisen, L., 1983. Physical responses to nutrient limitation. Annu. Rev. Microbiol. 37, 1–23.

Hein, J.R., Clague, D.A., Koski, R.A., Embley, R.W., Duhnam, R.E., 2008. Metalliferous sediment and a silica-hematite deposit within the Blanco Fracture Zone, Northeast Pacific. Mar. Georesour. Geotechnol. 26, 317–339.

Hekinian, R., Hoffert, M., Larque, P., Chemine, J.L., Stoffers, P., Bideau, D., 1993. Hydrothermal Fe and Si oxyhydroxide deposits from South Pacific intraplate volcanoes and East Pacific Rise axial and off-axial regions. Econ. Geol. 88, 2099–2121.

Herrington, R., Zaykov, V.V., Maslennikov, V.V., Brown, D., Puchkov, V.N., 2005. Mineral deposits of the Urals and Links to Geodynamic Evolution. Econ.Geol. 100th Anniiv. Vol. pp. 1069–1095.

Herzig, P.M., Hannington, M.D., Scott, S.D., Maliotis, G., Rona, P.A., Thompson, G., 1991. Gold-rich sea-floor gossans in the Troodos ophiolite and on the Mid-Atlantic ridge. Econ. Geol. 86, 1747–1755.

Himmler, T., Brinkmann, F., Bohrmann, G., Peckmann, J., 2011. Corrosion patterns of seep-carbonates from the eastern Mediterranean Sea. Terra Nova 23, 206–212.

Hoefs, J., 1997. Stable Isotope Geochemistry. Springer-Verlag, Berlin, Heidelberg, New York, London, Paris, Tokyo, Hong Kong (200 pp.).

Hollis, S.P., Cooper, M.R., Herrington, R.J., Roberts, S., Earls, G., Verbeeten, A., Piercey, S.J., Archibald, S.M., 2015. Distribution, mineralogy and geochemistry of silica-iron exhalites and related rocks from the Tyrone Igneous Complex: implications for VMS mineralization in Northern Ireland. J. Geochem. Explor. 159, 148–168.

Holm, N.G., 1988. Carbon isotope distribution in organic matter and siderite of modern metalliferous hydrothermal sediment and possible implications for gold associated with banded iron formation. Mar. Geol. 84, 201–207.

Hrischeva, E., Scott, S.D., 2007. Geochemistry and morphology of metalliferous sediments and oxyhydroxides from the Endevaur segment, Juan de Fuca Ridge. Geochim. Cosmochim. 71, 3476–3497.

Ivarsson, M., Bengtson, S., Belivanova, V., Stampanoni, M., Marone, F., Tehler, A., 2012. Fossilized fungi in subseafloor Eocene basalts. Geology 40, 163–166.

Jaffrés, J.B.D., Shields, G.A., Wallmann, K., 2007. The oxygen isotope evolution of seawater: A critical review of a long-standing controversy and an improved geological water cycle model for the past 3.4 billion years. Earth-Sci. Rev. 83, 83–122.

Jain, A., Loeppert, R.H., 2004. Effect of competing anions on the adsorption of arsenate and arsenite by ferrigydrite. J. Environ. Qual. 29, 1422–1430.

Jeong, B.C., Hawes, C., Bonthrone, K.M., Macaskie, L.E., 1997. Localization of enzymically enhanced heavy metal accumulation by Citrobacter sp. and metal accumulation in vitro by liposomes containing entrapped enzyme. Microbiology 143, 2497–2507.

Jin, Y.-G., Wang, H.-Y., Wang, W., 1991. Palaeoecological aspects of brachiopods from Chiungchussi Formation of early Cambrean age, eastern Yunnan, China. In: Jin, Y.G., et al. (Eds.), Palaeoecology of China v. 1. Nanjing University press, pp. 25–47.

Juniper, S.K., Fouquet, Y., 1988. Filamentous iron-silica deposits from modern and ancient hydrothermal sites. Can. Mineral. 26, 859–869.

Juniper, S.K., Jonnasson, I.R., Tunnicliffe, V., Southward, A.J., 1992. Influence of tube building polychaete on hydrothermal chimney mineralization. Geology 20, 895–898.

Kalogeropoulos, S.I., Scott, S.D., 1983. Mineralogy and geochemistry of tuffaceous exhalites (tetsusekiei) of the Fukazawa mine, Hokuroku district, Japan. Econ. Geol. Monogr. 5, 412–432.

Kashiwabara, T., Takahashi, Y., Marcus, M.A., Uruga, T., Tanida, H., Terada, Y., Usui, A., 2013. Tungsten species in natural ferromanganese oxides related to its different behavior from molybdenum in oxic ocean. Geochim. Cosmochim. Acta 106, 364–378.

Kelts, K., McKenzie, J.A., 1982. Diagenetic dolomite formation in Quaternary anoxic diatomaceous muds of DSDP Leg 64, Gulf of California. Initial Reports of the Deep Sea Drilling Project, pp. 553–569.

Kenter, J.A.M., 1989. Applications of computerized tomography in sedimentology. Mar. Geotechnol. 8, 201–211.

Kim, S.-T., O'Neil, J.R., 1997. Equilibrium and nonequilibrium oxygen isotope effects in synthetic carbonates. Geochim. Cosmochim. Acta 61, 3461–3475.

Kim, J., Dong, H., Seabaugh, J., Newell, S.W., Eberl, D.D., 2004. Role of microbes in the smectite-to-illite reaction. Science 303, 830–832.

Kletzin, A., Adams, M.W., 1996. Tungsten in biological systems. FEMS Microbiol. Rev. 18 (1), 5–63.

Konhauser, K., 2006. Introduction to Geomicrobiology. Blackwell Publ., Maldon (425 pp.).

Kopp, R.E., Kirschvink, J.L., 2008. The identification and biogeochemical interpretation of fossil magnetotactic bacteria. Earth Sci. Rev. 86, 42–61.

Krajewski, K.P., Van Cappellen, P., Trichet, J., Kuhn, O., Lucas, J., Martı'n-Algarra, A., Pre'vo^t, L., Tewari, V.C., Gaspar, L., Knight, R.I., Lamboy, M., 1994. Biological processes and apatite formation in sedimentary environments. Eclogae Geol. Helv. 87, 701–745.

Kranidiotis, P., Maclean, W.H., 1987. Systematics of Chlorite Alteration at the Phelps Dodge Massive Sulfide Deposit, Matagami, Quebec. Econ. Geol. 82, 1898–1911.

Lein, A.Y., Sedykh, E.M., Starshinova, N.P., 1989. Distribution of metals in bacteria and animals from submarine hydrothermal fields. Geochim. Int. 2, 297–303.

Little, C.T.S., Maslennikov, V.V., Morris, N.J., Gubanov, A.P., 1999. Two Paleozoic hydrothermal vent communities from the southern Ural Mountains, Russia. Palaeontology 42, 1043–1078.

Little, C.T.S., Glynn, S.E.J., Mills, R.A., 2004. Four-Hundred-and-Ninety-million year record of bacteriogenic iron oxide precipitation at sea-floor hydrothermal vent. Geomicrobiol J. 21, 415–429.

Lowenstam, H.A., Weiner, S., 1989. On Biomineralization. Oxford University Press, New York 324 pp.

Lyonsa, T.W., Werneb, J.P., Hollanderb, D.J., Murray, R.W., 2003. Contrasting sulfur geochemistry and Fe/Al and Mo/Al ratios across the last oxic-to-anoxic transition in the Cariaco Basin, Venezuela. Chem. Geol. 195, 131–157.

Manning, B.A., Goldberg, S., 1996. Modeling Competitive Adsorption of Arsenate with Phosphate and Molybdate on Oxide Minerals. Soil Sci. Soc. Am. J. 60, 121–131.

Maslennikov, V.V., 1999. Sedimentogenesis, halmyrolysis and ecology of the massive sulfide paleohydrothermal fields (on the example of the Southern Urals). Geotur, Miass (348 pp. *(in Russian with English abstract)*.

Maslennikov, V.V., 2006. Lithogenesis and massive sulfide deposits formation. Institute of Mineralogy UB RAS press, Miass (384 pp. *(in Russian with English abstract)*.

Maslennikov, V.V., Ayupova, N.R., Herrington, R.J., Danyushevskiy, L.V., Large, R.R., 2012. Ferruginous and manganiferous haloes around massive sulphide deposits of the Urals. Ore Geol. Rev. 47, 5–41.

Maslennikov, V.V., Maslennikova, S.P., Large, R.R., Danyushevskiy, L.V., Herrington, R.J., Stanley, C.J., 2013. Tellurium-bearing minerals in zoned sulfide chimneys from Cu-Zn massive sulfide deposits of the Urals, Russia. Mineral. Petrol. 107, 67–99.

Maslennikov, V.V., Ayupova, N.R., Maslennikova, S.P., Tret'yakov, G.A., Melekestzeva, I.Y., et al., 2014. Toxic elements in massive sulfide systems. RIO UB RAS press, Yekaterinburg (245 pp. *(in Russian)*.

Maslennikov, V.V., Ayupova, N.R., Maslennikova, S.P., Lein, A.Y., Thelyko, A.S., Danyushevskiy, L.V., Large, R.R., 2016. The criteria for detection of hydrothermal vent fauna in massive sulfide deposits of Urals. Lithol. Miner. Resour. in press.

Maslennikov, V.V., Maslennikova, S.P., Large, R.R., Danyushevskiy, L.V., Herrington, R.J., Aupova, N.R., Zaykov, V.V., Lein, A.Y., Tseluyko, A.S., Melekestseva, I.Y., Tessalina, S.G., 2017. Chimneys in paleozoic massive sulfide mounds of the Urals VMS deposits: mineral and trace element comparison with modern black, gray and clear smokers. Ore Geol. Rev. 85, 64–106 (in this issue).

Maslennikova, S.P., Maslennikov, V.V., 2007. Paleozoic "black smoker" sulfide chimneys (after the example of Ural). UB RAS, Ekaterinburg (312 pp. *(in Russian with English abstract)*.

Maynard, J.B., 1983. Geochemistry of sedimentary ore deposits. Springer-Verlag, New York-Heidelberg–Berlin 305 pp.

Melekestseva, I.Y., Tret'yakov, G.A., Nimis, P., Yuminov, A.M., Maslennikov, V.V., Maslennikova, S.P., Kotlyarov, V.A., Beltenov, V.E., Danyushevsky, L.A., Large, R., 2014. Barite-rich massive sulfides from the Semenov-1 hydrothermal field (Mid-Atlantic Ridge, 13 degrees 30.87′ N): Evidence for phase separation and magmatic input. Mar. Geol. 349, 37–54.

Mills, R.A.J., Thomson, H., Elderfield, R.W., Hinton, R.W., Hyslop, E., 1994. Uranium enrichment in metalliferous sediments from the Mid-Atlantic Ridge. Earth Planet. Sci. Lett. 124, 35–47.

Morad, S., 1988. Diagenesis of titaniferous minerals in Jurassic sandstones from the Norwegian Sea. Sediment. Geol. 57, 17–40.

Morin, G., Juillot, F., Casiot, C., Bruneel, O., Persone, J.-C., Elbazpoulichet, F., Leblanc, M., Ildefonse, P., Calas, G., 2003. Bacterial formation of tooeleite and mixed arsenic (III) or arsenic (V) – iron (III) gels in the Carnoules acid mine drainage, France. A XANES, XRD, and SEM study. Environ. Sci. Technol. 37, 1705–1712.

Muehlenbachs, K., Furnes, H., Fonneland, H.C., Hellevang, B., 2003. Ophiolites as faithful records of the oxygen isotope ratio of ancient seawater: the Solund-Stavfjord ophiolite complex as a Late Ordovician example. In: Dilek, Y., Robinson, P.T. (Eds.), Ophiolites in Earth History. Geol. Soc. London Spec. Pub Vol. 218, pp. 401–414.

Needham, S.J., Worden, R.H., McIlroy, D., 2004. Animal-sediment interactions: the effect of ingestion and excretion by worms on mineralogy. Biogeosciences 1, 113–121.

Orians, K.J., Boyle, E.A., Bruland, K.W., 1990. Dissolved titanium in the open ocean. Nature 348, 322–325.

Pactung, D., Foster, A., Laflamme, G., 2003. Speciation and characterization of arsenic in Ketza River mine tailings using X-ray adsorptoin spectroscopy. Environ. Sci. Technol. 37, 2067–2074.

Peter, J.M., Goodfellow, W.D., 1996. Mineralogy, bulk and rare earth element geochemistry of massive sulphide-associated hydrothermal sediments of the Brunswick horizon, Bathurst mining camp, New Brunswick. Can. J. Earth Sci. 33, 252–283.

Picard, A., Kappler, A., Schmid, G., Quaroni, L., Obst, M., 2015. Experimental diagenesis of organo-mineral structures formed by microaerophilic Fe(II)-oxidizing bacteria. Nat. Commun. 18 (6), 6227.

Polgári, M., Hein, J.R., Vigh, T., Szabó-Drubina, M., Fórizs, I., Bíró, L., Müller, A., Tóth, A.L., 2012. Microbial processes and the origin of the Úrkút manganese deposit, Hungary. Ore Geol. Rev. 47, 87–109.

Pracejus, B., Halbach, P., 1996. Do marine moulds influence Hg and Si precipitation in the hydrothermal JADE field (Okinawa Trough)? Chem. Geol. 130, 87–99.

Prokin, V.A., Buslaev, F.P., 1999. Massive copper-zinc sulphide deposits in the Urals. Ore Geol. Rev. 14, 1–69.

Rahman, A., Hassler, C., 2014. Is arsenic biotransformation a detoxification mechanism for microorganism? Aquat. Toxicol. 146, 212–219.

Reitner, Y., 1993. Modern cryptic microbialite/metazoan facies from Lizard Island (Great Barrier Reef, Australia). Facies 29, 3–39.

Rieger, R.M., Purschke, G., 2005. The coelom and the origin of the annelid body plan. Hydrobiologia 535, 127–137.

Sagemann, J., Bale, S.J., Briggs, D.E.G., Parkes, R.J., 1999. Controls on the formation of authigenic minerals in association with decaying organic matter: an experimental approach. Geochim. Cosmochim. Acta 63, 1083–1095.

Schmittner, K.-E., Giresse, P., 1999. Micro-environmental controls on biomineralization: superficial processes of apatite and calcite precipitation in Quaternary soils, Roussillon, France. Sedimentology 46, 463–476.

Shi, C., Cao, J., Hu, K., Bian, L., Yao, S., Zhou, J., Han, S., 2014. New understandings of Ni–Mo mineralization in early Cambrian black shales of South China: Constraints from variations in organic matter in metallic and non-metallic intervals. Ore Geol. Rev. 59, 73–82.

Shillito, B., Lechaire, J.-P., Goffinet, G., Gaill, F., 1995. Composition and morphogenesis of the tubes of vestimentiferan worms. In: Parson, L.M., Walker, C.L., Dixon, D.R. (Eds.), Hydrothermal Vents and Processes. Geological Society (London) Special Publication Vol. 87, pp. 295–302.

Singer, P.C., Stumm, W., 1970. Acidic mine drainage: the rate-determining step. Science 167, 1121–1123.

Slack, J.F., Jiang, W.-T., Peacor, D.R., Okita, P.M., 1992. Hydrothermal and metamorphic berthierine from the Kidd Creek volcanogenic massive sulfide deposit. Can. Mineral. 30, 1127–1142.

Søgaard, E.G., Medenwaldt, R., Abraham-Peskir, J.V., 2000. Conditions and rates of biotic and abiotic iron precipitation in selected Danish fresh water plants and microscopic analysis of precipitate morphology. Water Res. 34, 2675–2682.

Sposito, G., 1984. The surface chemistry of soils. Oxford Univ. Press, London (234 pp.).

Stetter, K.O., Fiala, G., Huber, G., Ruber, R., Segerer, A., 1990. Hyperthermophilic microorganisms. FEMS Microbiol. Rev. 75, 117–124.

Thorseth, I.H., Furnes, H., Tumyr, O., 1995. Textural and chemical effects of bacterial activity on basaltic glass: an experimental approach. Chem. Geol. 119, 139–160.

Tornos, F., Solomon, M., Conde, C., Spiro, B., 2008. Formation of the Tharsis Massive Sulfide Deposit, Iberian Pyrite Belt: Geological, Lithogeochemical, and Stable Isotope Evidence for Deposition in a Brine Pool. Econ. Geol. 103, 185–214.

Tornos, F., Peter, J.M., Allen, R., Conde, C., 2015. Controls on the siting and style of volcanogenic massive sulphide deposits. Ore Geol. Rev. 68, 142–163.

Torsvik, T., Furnes, H., Muehlenbachs, K., Thorseth, I., Tumyr, H.O., 1998. Evidence for microbial activity at the glass–alteration interface in oceanic basalts.Earth Planet. Sci. Lett. 162, 165–176.

Ulrich, H.J., Stone, A.T., 1989. Oxidation of chlorophenols adsorbed to manganese oxide surfaces. Environ. Sci. Technol. 23, 421–428.

Vasconcelos, C., McKenzie, J.A., Bernasconi, S., Grujic, D., Tien, A.J., 1995. Microbial mediation as a possible mechanism for natural dolomite formation at low temperatures. Nature 377, 220–222.

Vinn, O., Mutvei, H., 2009. Calcareous tubeworms of the Phanerozoic. Est. J. Earth Sci. 58, 286–296.

Watson, E.B., 1996. Surface enrichment and trace-element uptake during crystal growth. Geochim. Cosmochim. Acta 60, 5013–5020.

Wolfe-Simon, F., Blum, J.S., Kulp, T.R., Gordon, G.W., Hoeft, S.E., Pett-Ridge, J., Stolz, J.F., Webb, S.M., Weber, P.K., Davies, P.C.W., Anbar, A.D., Oremland, R.S., 2010. Science 332 (6034), 1163–1166.

Yapp, C.J., Poths, H., 1986. Carbon in natural goethites. Geochim. Cosmochim. Acta 50, 1213–1220.

Zaykov, V.V., 2006. Volcanism and sulfide mounds of paleocean margins (after the example of Ural's and Siberia's massive sulfide-bearing zones). Nauka press, Moscow (428 pp. *(in Russian with English abstract)*.

Zaykov, V.V., Maslennikov, V.V., Zaykova, E.V., Herrington, R.J., 2002. Ore-formational and ore–facial analysis of the massive sulfide deposits of the Uralian paleoocean. Institute of Mineralogy press, Miass (315 pp. *(in Russian)*.

Zhu, M.-Y., Zhang, J.-M., Li, G.-X., 2001. Sedimentary environments of the early Cambrian Chengjiang Biota: sedimentary of the Yu'anshan Formation in Chengjiang Country, eastern Yunnan. Acta Palaeontol. Sin. 40, 80–105.

Zhu, J., Pigna, M., Cozzolino, V., Caporale, A.G., Violante, A., 2011. Sorption of arsenite and arsenate on ferrihydrite.Effect of organic and inorganic ligands. J. Hazard. Mater. 189, 564–571.